



1 **Anomalous summertime CO₂ sink in the subpolar Southern**
2 **Ocean promoted by early 2021 sea ice retreat**

3 Kirtana Naëck^{1*}, Jacqueline Boutin¹, Sebastiaan Swart², Marcel du Plessis², Liliane Merlivat¹,
4 Laurence Beaumont³, Antonio Lourenco¹, Francesco d'Ovidio¹, Louise Rousselet¹, Brian
5 Ward⁴, Jean-Baptiste Sallée¹

6 ¹ Sorbonne Université, CNRS, IRD, MNHN, Laboratoire d'Océanographie et du Climat : Expérimentations et
7 Approches Numériques, LOCEAN/IPSL, F-75005 Paris, France

8 ²Department of Marine Sciences, University of Gothenburg, Sweden

9 ³DT-INSU Meudon, France

10 ⁴University of Galway, Ireland

11 * Correspondence to: kirtana.naeck@locean.ipsl.fr and jacqueline.boutin@locean.ipsl.fr

12 **Abstract**

13 The physical and biogeochemical processes governing the air-sea CO₂ flux in the Southern Ocean are still widely
14 debated. The “Southern Ocean Carbon and Heat Impact on Climate” cruise in summer 2022 aimed at studying
15 these processes in the Weddell Sea and in its vicinity. A “CARbon Interface OCean Atmosphere” (CARIOCA)
16 drifting buoy was deployed in January 2022 in the subpolar Southern Ocean, providing hourly surface ocean
17 observations of fCO₂ (fugacity of CO₂), dissolved oxygen, salinity, temperature and chlorophyll-a fluorescence for
18 17 months. An underwater glider was piloted with the buoy for the first 6 weeks of the deployment to provide
19 vertical ocean profiles of hydrography and biogeochemistry. These datasets reveal an anomalously strong ocean
20 carbon sink for over 2 months occurring in the region of Bouvet Island and associated with large plumes of
21 chlorophyll-a (Chl-a). Based on Lagrangian backward trajectories reconstructed using various surface currents
22 fields, we identified that the water mass reaching the Bouvet Island region originated from the south-west, from
23 the vicinity of sea ice edge in spring 2021. We suggest that a strong phytoplankton bloom developed there in
24 November 2021 through dissolved iron supplied by early sea ice melt in 2021 in the Weddell Sea. These waters,
25 depleted in carbon, then travelled to the position of the CARIOCA buoy. The very low values of ocean fCO₂,
26 measured by the buoy (down to 310 µatm), are consistent with net community production previously observed
27 during blooms occurring near the sea ice edge, partly compensated by air-sea CO₂ flux along the water mass
28 trajectory. Early sea ice retreat might therefore have caused a large CO₂ sink farther north than usual in summer
29 2022, in the Atlantic sector of the subpolar Southern Ocean. Such events might become more frequent in the future
30 as a result of climate change.

31



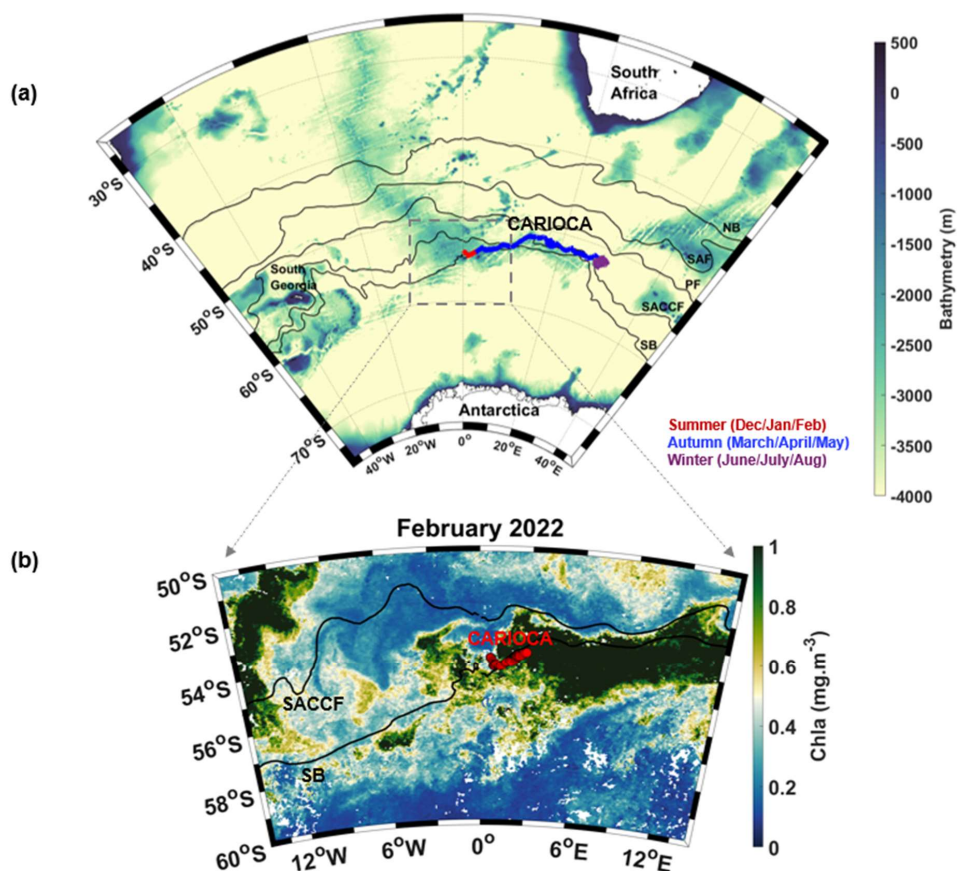
32 1. Introduction

33 According to the latest Global Carbon Budget, atmospheric CO₂ concentrations keep increasing and are projected
34 to be 51% higher than pre-industrial levels in 2023. The ocean helps mitigate the atmospheric CO₂ increase by
35 acting as a carbon sink. Indeed, during the past decade (2013-2022), the global ocean absorbed $2.9 \pm 0.4 \text{ GtC yr}^{-1}$,
36 representing 26% of worldwide CO₂ emissions annually (Friedlingstein et al., 2023). The Southern Ocean plays
37 an important role in the ocean's buffering capacity. Defined as the ocean surrounding Antarctica, south of 30-35°
38 S, it covers only about 20-30% of the global ocean surface, yet serves as a main pathway for anthropogenic carbon
39 uptake (Frölicher et al., 2015; Gruber et al., 2019). It is, in fact, responsible for about 40% of the global oceanic
40 uptake of anthropogenic CO₂ (DeVries, 2014; Frölicher et al., 2015; Gruber et al., 2019; Mayot et al., 2023).

41 The direction of the air-sea CO₂ flux is determined by the difference between the fugacity of CO₂ at the ocean
42 surface, $f\text{CO}_2$, and in the atmosphere, $f\text{CO}_{2\text{atm}}$. When the $f\text{CO}_2$ is undersaturated with respect to the atmosphere,
43 the ocean is a carbon sink (Wanninkhof, 2014). Any process that affects $f\text{CO}_2$ at local or regional scale, like the
44 biological activity, or the ocean circulation, can therefore affect the ocean carbon pump (Henley et al., 2020).
45 Ultimately, it is the balance between the biological pump, the solubility pump, and ocean circulation which will
46 determine whether the surface ocean will behave as a sink or a source of carbon to the atmosphere.

47 The lack of $f\text{CO}_2$ observations have posed a daunting challenge to the ocean community to understand the full
48 suite of mechanisms controlling the air-sea CO₂ flux, and to assess its net magnitude. This is particularly true in
49 the Southern Ocean, which is renowned to be pivotal in controlling global air-sea CO₂ flux, but is also one of the
50 regions suffering the most from $f\text{CO}_2$ observation scarcity. As a result, there are large discrepancies in the Southern
51 Ocean carbon sink estimates from the literature, which result in large uncertainties in our global estimates of air-
52 sea CO₂ flux (Friedlingstein et al., 2023). The difficulty to assess CO₂ uptake by the Southern Ocean is exacerbated
53 by the fact that this basin has a large interdecadal variability, and that observation-based products, such as those
54 derived from SOCAT (Bakker et al., 2016), and Global Ocean Biogeochemical Models (GOBMs) have shown
55 different interannual trends for the past years. In this regard, a better understanding of the different processes
56 governing the air-sea flux of CO₂ is essential in order to anticipate the effects of climate change on the Southern
57 Ocean's capacity to continue sequestering carbon (Hauck et al., 2023; Mayot et al., 2023; Meijers et al., 2023).

58 The SO-CHIC ("Southern Ocean Carbon and Heat Impact on Climate") European programme was launched to
59 tackle this knowledge gap (The SO-CHIC consortium et al., 2023). In this context, during the *S.A. Agulhas II*
60 summer research cruise in January 2022 (Ward et al., 2022), a CARIOCA ("CARbon Interface Ocean
61 Atmosphere") buoy was deployed near the Southern Boundary, north-east of the Weddell Sea, and west of Bouvet
62 Island (Naëck et al., 2024). At the same time, an underwater ocean glider (675) (Swart et al., 2024), alongside deep
63 CTD sections (Steiger et al., 2022) were deployed. The glider followed the buoy for six weeks to provide
64 observations of the underlying ocean conditions. The CARIOCA buoy acquired $f\text{CO}_2$ measurements in the
65 subpolar region (Fig 1) where surface $f\text{CO}_2$ observations have been sparse in the past twenty years (Gruber et al.,
66 2019).



67

68 **Figure 1: (a) CARIOCA trajectory from 26 January 2022 to 27 June 2022 superimposed on a bathymetry map of the**
69 **study zone. Fronts from Park & al. 2019 are indicated, from north to south: Northern Boundary (NB) of the ACC,**
70 **Subantarctic Front (SAF), Polar Front (PF), Southern Antarctic Circumpolar Current Front (SACCf) and Southern**
71 **Boundary (SB) of the ACC. (b) CCI Chl-a map with CARIOCA trajectory in February.**

72 In this paper, we use these unique field observations to investigate the cause of fCO₂ variations along the trajectory
73 of the buoy, with a particular focus on the role of biological activity in shaping these variations. The Southern
74 Ocean is a High Nutrient Low Chlorophyll (HNLC) region, with iron as the key limiting nutrient for phytoplankton
75 growth. Sources of iron to the ocean mixed layer therefore condition the efficiency of the biological carbon pump.
76 Iron can come from island/plateau sources, ocean ridge sources or from an sea ice source (Ardyna et al., 2019). In
77 summer 2022, west and north-east of Bouvet Island (54.42 °S 3.34 °E, Fig. 1), an unusually large CO₂ sink was
78 observed along the path of the buoy, as well as high biological activity. This study aims to investigate the processes
79 that contributed to this summer 2022 large CO₂ sink. In the next section the instruments deployed, the different
80 data sets and the methodology used will be described. There will then be a description of the results followed by
81 a discussion.



82 2. Materials and methods

83 2.1 CARIOCA measurements

84 The CARIOCA buoy was deployed on 24 January 2022 at 54°S, 0°W. It was anchored at 15 m depth and followed
85 the currents in a quasi-Lagrangian way. A three-wavelength spectrophotometer (434, 596 and 830 nm) was used
86 to measure $f\text{CO}_2$. The $f\text{CO}_2$ sensor included an exchanger where a dye solution (thymol blue) was brought into
87 equilibrium with seawater via a semi-permeable CO_2 membrane. The absorption coefficient of the dye was
88 measured by the spectrophotometer and was then related to the carbonate properties of seawater. The three-
89 wavelength measurements enable correction of any modification of the optical path or of the opacity of the optical
90 cell (Copin-Montégut et al., 2004). The absolute precision of the $f\text{CO}_2$ is estimated $\pm 3 \mu\text{atm}$ and its relative
91 precision is $\pm 1 \mu\text{atm}$. A thermosalinograph measured the sea surface temperature at 2 m depth, SST, and the
92 conductivity, from which sea surface salinity, SSS, was derived. An optode measured dissolved oxygen (O_2).
93 According to the manufacturer, the precision of the O_2 measurements is $\sim 8 \mu\text{mol L}^{-1}$ (5 %). Calibrated values
94 were given by the manufacturer for pure water and they were corrected from the effects of temperature and salinity
95 as described in Merlivat et al. (2015). A fluorometer measured the fluorescence which was calibrated in Chl-a
96 units using the calibrated Seaglider (675) fluorescence (see section 2.3). An anemometer measured wind speed
97 and a barometer measured atmospheric pressure (Patm) at 2 m above the sea surface. The wind at 10 m above the
98 ocean was derived assuming a neutral atmosphere. As from 4 June 2022, the CARIOCA atmospheric sensor
99 stopped working, and the wind and atmospheric pressure data were replaced with data from ERA5 (C3S, 2018).
100 During their common period, CARIOCA and colocated ERA5 data were very similar (mean difference = 0.26 m
101 s^{-1} , $R^2 = 0.86$, not shown). The buoy acquired 17 months of data which was transmitted in real time via ARGOS,
102 and stopped functioning on the 24 June 2023. In this study, we only use observations from the period of 26 January
103 2022 to 27 June 2022, which corresponds to the time during which a strong CO_2 sink was observed.

104 2.2 CARIOCA derived parameters

105 The air-sea flux of CO_2 represents the exchanges of CO_2 at the ocean-atmosphere interface. This air-sea flux of
106 CO_2 (F) was calculated using Wanninkhof's methodology (Wanninkhof, 1992, 2014).

$$107 F = K (f\text{CO}_{2\text{ssw}} - f\text{CO}_{2\text{atm}}) \quad (1)$$

108 where $f\text{CO}_{2\text{ssw}}$ and $f\text{CO}_{2\text{atm}}$ are the fugacity of CO_2 at the ocean surface and in the atmosphere and K is the CO_2
109 exchange coefficient (Wanninkhof, 1992). The $f\text{CO}_{2\text{atm}}$ was determined using atmospheric CO_2 concentration data
110 ($x\text{CO}_2 \text{ atm}$) from SPO ("South Pole Antarctica"), and CARIOCA Patm according to Eqn. 2 in Boutin et al. (2008).
111 To eliminate $f\text{CO}_2$ changes linked to temperature and salinity, the concentration of dissolved inorganic carbon
112 (DIC) was estimated. At given SST and SSS, the DIC and alkalinity was estimated from $f\text{CO}_2$. The alkalinity was
113 calculated according to Lee et al. (2006). The Matlab routine *CO2SYS*, with dissociation constants K_1 and K_2 of
114 Lueker et al. (2000) was used to derive DIC. Oxygen saturation ($\text{O}_{2\text{sat}}$), the degree of oxygen saturation ($p\text{O}_{2\text{sat}}$)
115 and the oxygen flux at the air-sea interface (FO_2) were calculated as per Merlivat et al. (2015). The oxygen anomaly
116 was calculated by subtracting the dissolved oxygen concentration calculated at saturation from the dissolved
117 oxygen concentration ($\text{O}_2 - \text{O}_{2\text{sat}}$). During photosynthesis, a positive anomaly is expected whereas during respiration
118 / remineralization, a negative anomaly is expected. The oxygen measurements of the CARIOCA drifter could not
119 be recalibrated at sea, because unfortunately the O_2 measured by the CTD at the deployment was not calibrated.



120 An empirical correction of $+8 \mu\text{mol/kg}$ (which corresponds to the precision of the optode) was applied to bring the
121 values of $\text{O}_2 - \text{O}_{2\text{sat}}$ above zero, during periods of high biological activity. These high biological periods are detected
122 from CARIOCA fluorescence and opposite variations in O_2 and DIC. The carbon net community production,
123 NCPc, and the oxygen net community production, NCPo_2 , were estimated during periods of high biological
124 activity, during which diurnal cycles with DIC and $\text{O}_2 - \text{O}_{2\text{sat}}$ in opposition were observed by the CARIOCA buoy,
125 following the same methodology as in Merlivat et al. (2015), using mixed layer depth (MLD) derived from glider
126 vertical profiles (see section 2.3).

127 **2.3 Seaglider measurements and derived parameters**

128 The Seaglider (SG675) followed the CARIOCA buoy for a month and a half, from 31 January 2022 to 10 March
129 2022 (39 days) (Fig. 1), providing vertical profiles of temperature, salinity, oxygen and fluorescence of the upper
130 1000 m of the water column. There was a time lapse of about one day between CARIOCA and the glider, the
131 glider being about one day behind the buoy each time. Both instruments were less than 20 km apart during that
132 period. For this study, only profiles between the 31 January and the 10 March 2022 were considered, which was
133 when the glider and the CARIOCA were nearest to each other. The glider data was processed using the
134 “GliderTools” package (Gregor et al., 2019; Swart et al., 2024). For the salinity data, outliers and spikes were
135 removed and a smoothing was applied with Savitzky-Golay filter. The glider salinity data was also validated using
136 the CTD salinity profile at the time of deployment (on the 23 January 2022 14h46). The CTD salinity data had
137 already been calibrated, and the CARIOCA SSS data was in turn validated using the already validated glider
138 surface salinity data. The glider salinity at 2 m and the CARIOCA SSS (at 2 m), were in good agreement, with a
139 small difference of about 0.05 pss. Using “GliderTools”, the glider fluorescence profiles were also quality
140 controlled. Outliers, spikes and bad profiles were removed, and the data was corrected for in situ dark counts. A
141 quenching correction using the same method as Thomalla et al., 2018 was applied. The glider fluorescence was
142 calibrated and converted to chlorophyll-a using the CTD fluorescence at the time of deployment.

143 The mixed layer depth, MLD, was estimated using the glider data using the density threshold of 0.03 kg m^{-3} (de
144 Boyer Montégut et al., 2004)). It has been observed in past studies that DIC can be more sensitive to the mixing
145 layer, XLD, which can be determined using turbulence measurements (Nicholson et al., 2022; Pellichero et al.,
146 2020; Sutherland et al. 2014; Giunta and Ward 2022). The empiric relationship approximated by Nicholson et al.
147 (2022) was used to estimate XLD. (The MLD and the XLD are surface layers directly influenced by the
148 atmosphere. The MLD has homogenised, formed as a result of mixing, while the XLD is still actively influenced
149 by turbulence and still mixing).

150 **2.4 S.A. Agulhas II TSG**

151 The S.A. *Agulhas II* was equipped with a thermosalinograph (TSG) (Ward et al., 2024), and ship measurements
152 of salinity and temperature were collected, from South Africa to Antarctica, and back again, from the 3 December
153 2021 to the 28 January 2022. The S.A. *Agulhas II* TSG SSS data was calibrated using underway water samples
154 collected during the SO-CHIC cruise (Ward et al., 2022).



155 **2.5 Satellite, analysis, and reanalysis datasets**

156 Chlorophyll-a satellite images are from the Climate Change Initiative product version 6.0 (OceanColour - CCI,
157 2024), from 1997 to 2022, for spring (November: 1997-2020) and summer (January, February: 1998-2022).
158 Monthly and weekly means were used for the Chl-a. For the surface salinity data, Glorys reanalysis (Global Ocean
159 Physics Reanalysis, 2024), Mercator analysis (Global Ocean Physics Analysis and Forecast, 2024) at 5 m depth,
160 SMOS CATDS CECv9.0 (18 days) satellite data (Boutin et al., 2023) and ISAS analysis at 5 m depth (In Situ
161 Analysis System, an optimal interpolation from ARGO floats) (Szekely et al., 2024) were used. A colocalization
162 between Mercator / Glorys salinity data and CARIOCA SSS indicates that both datasets were in good agreement,
163 showing similar patterns, but with Mercator / Glorys salinity data being lower than the CARIOCA by about 0.1
164 pss from February 2022 to mid-April 2022 (Fig. B1 in Appendix).

165 Daily and monthly data, from Mercator analysis were used as of July 2021, and Glorys reanalysis was used for the
166 years before July 2021. The Mercator/Glorys products were also used to analyse vertical salinity and surface
167 current velocities. Sea ice data was obtained from OSI SAF (EUMETSAT - Product Navigator - Global Sea Ice
168 Concentration Climate Data Record v3.0 - Multimission, 2024; EUMETSAT - Product Navigator - Global Sea Ice
169 Concentration Interim Climate Data Record Release 3 - DMSP, 2024).

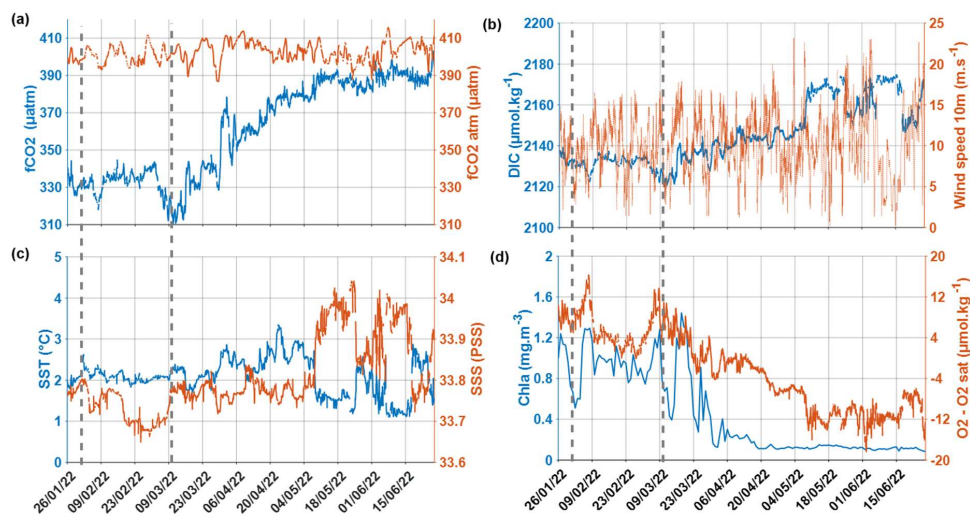
170 **2.6 Lagrangian analysis**

171 Backward trajectories of water masses were computed with a Lagrangian analysis (Sergi et al., 2020) using the
172 LAMTA software (Rousselet, L et al., 2024 pre-print). After initialising the particles at specific dates, longitudes
173 and latitudes, a backward advection was performed to estimate the trajectories of these particles several months
174 before. To determine which water masses reached the CARIOCA, particles were initialised at the CARIOCA
175 coordinates, with one coordinate point per hour (i.e. 24 points advected backwards in time each day). Three current
176 products were tested, namely, GlobCurrent (Global Total (COPERNICUS-GLOBCURRENT), Ekman and
177 Geostrophic currents at the Surface, 2024), Mercator Analysis (Global Ocean Physics Analysis and Forecast, 2024)
178 / Glorys reanalysis (Global Ocean Physics Reanalysis, 2024) and OSCAR (OSCAR third degree resolution ocean
179 surface currents | PO.DAAC / JPL / NASA, 2024). Using Mercator analysis / Glorys reanalysis, different depths
180 were also tested, namely 5 m, 15 m, 34 m and 55 m. Using OSCAR, the backward trajectories in November,
181 January and February were also computed, from 1997 to 2022. In the next sections, we are showing the results
182 obtained using the total currents, i.e. the sum of the geostrophic and Ekman currents, at 15 m depth. The reliability
183 of numerical trajectories for reconstructing phytoplanktonic blooms from nutrient sources and up to mesoscale
184 precision has been validated in the Southern Ocean from multi satellite data, surface drifters, and lithogenic
185 isotopes (Sergi et al. 2020; d'Ovidio et al. 2015; Sanial et al. 2014).

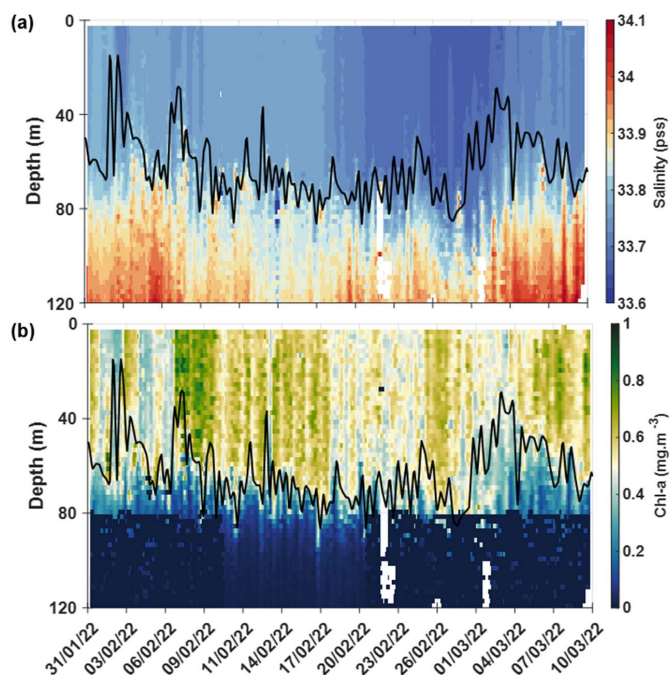


186 **3. Results**

187 **3.1 CARIOCA and Seaglider observations**



188
189 **Figure 2: CARIOCA time series from the 26 January to the 27 June 2022: (a) Atmospheric and surface ocean $f\text{CO}_2$**
190 **($f\text{CO}_{2\text{atm}}$ and $f\text{CO}_2$), (b) DIC and wind speed, (c) SST and SSS, (d) Chl-a and $\text{O}_2 - \text{O}_{2\text{sat}}$, with the period during which the**
191 **glider followed the buoy (31 January to 10 March 2022) indicated by dotted lines.**

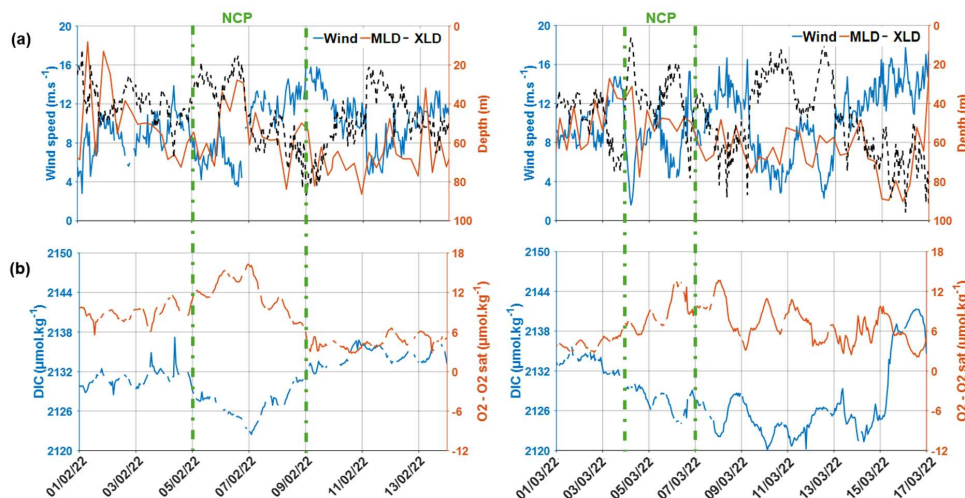


192
193 **Figure 3: Seaglider profile time series between the 31 January and the 10 March 2022 of (a) salinity, (b) Chl-a, with**
194 **the MLD indicated with the black line.**



195 Low surface salinities were measured in February 2022, both by the CARIOCA buoy (Fig. 2 (c)) and by the glider
196 (Fig. 3 (a)) with minimum values of salinity in the second half of February. The CARIOCA measured surface
197 salinities around 33.7 pss between 17 February and 8 March 2022. Both the glider and the CARIOCA observed
198 maximas of surface Chl-a around the 7 February and the 7 March 2022 (Fig. 2 (d) and Fig. 3 (b)). According to
199 the glider profiles, the low values of salinity, and high concentrations of Chl-a, observed from early February to
200 early March, were well mixed within the mixed-layer, confined to the top 60 m or so (Fig. 3). According to fig. 2
201 (a), a very low $f\text{CO}_2$ was observed by the CARIOCA in summer 2022, while the buoy was in this fresh water mass,
202 enriched in Chl-a and oxygen. The $\text{d}f\text{CO}_2$ is about $-60 \mu\text{atm}$ from the end of January to the end of March 2022.
203 Minima of $f\text{CO}_2$ ($\sim 320 \mu\text{atm}$) and of DIC ($\sim 2120 \mu\text{mol kg}^{-1}$) occurred on the 7 February and the 7 March 2022,
204 which also coincided with maximum concentrations of chlorophyll-a ($\sim 1.3 \text{ mg m}^{-3}$) and of oxygen. Around these
205 dates, diurnal cycles of DIC and $\text{O}_2\text{-O}_{2\text{sat}}$, with the DIC and $\text{O}_2\text{-O}_{2\text{sat}}$ in opposite phases were clearly observed, and
206 allowed NCP estimates (see next section). According to CARIOCA measurements (Fig. 2 (a)), after March, as the
207 CARIOCA drifted away from the phytoplankton bloom, $f\text{CO}_2$ started increasing, until it reached values close to
208 equilibrium with the atmosphere on 27 June 2022.

209 3.2 NCP and impact of wind on MLD



210
211 **Figure 4: CARIOCA time series, during NCP periods on the 5-9 February 2022 (left), and on the 4-7 March 2022**
212 **(right), (a) Wind speed, MLD and XLD (b) DIC and $\text{O}_2\text{-O}_2$ sat.**

213 During the two periods dominated by biological activity, on the 5-9 February 2022, and on the 4-7 March 2022,
214 Chl-a increased by 0.5 mg m^{-3} and DIC decreased by $10 \mu\text{mol kg}^{-1}$ (Fig.2, Fig. 4 and Fig. A1 in Appendix A). Just
215 before the peaks of Chl-a (corresponding to minimum concentrations of DIC and maximum concentrations of
216 oxygen), there were very low wind speeds, associated with a shoaling of the mixed layer (Fig. 2 and Fig. 4), which
217 itself might have enhanced Chl-a bloom at the surface (Fig. 3). During the February event, NCPc was estimated
218 to reach $-91 \text{ mmol m}^{-2} \text{ d}^{-1}$, while NCP_{O_2} was $132 \text{ mmol m}^{-2} \text{ d}^{-1}$. During the March event, NCPc of $-104 \text{ mmol m}^{-2} \text{ d}^{-1}$
219 and NCP_{O_2} of $138 \text{ mmol m}^{-2} \text{ d}^{-1}$ were estimated (Fig. A1 in Appendix). It is interesting to note that the two



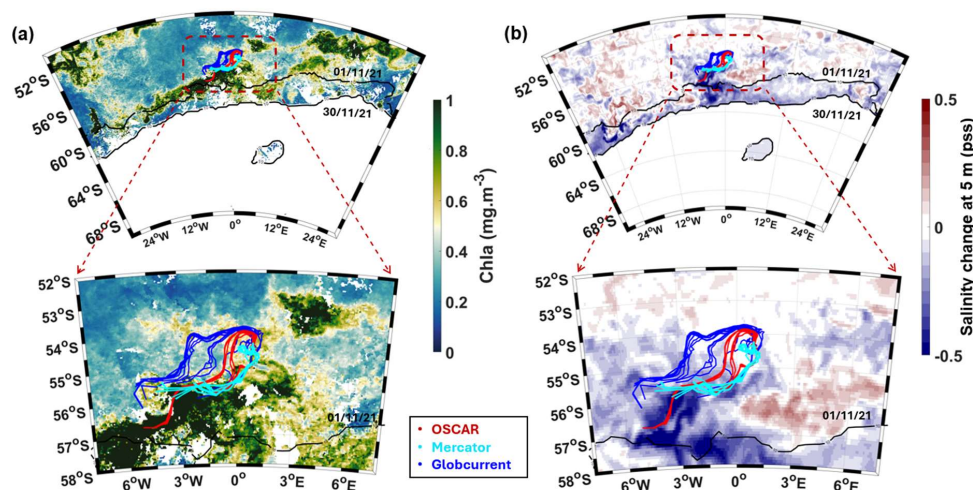
220 values of the photosynthetic quotient, $PQ = NCP_{O_2} / NCP_C$, respectively equal to 1.45 and 1.33 are in close good
221 agreement with the value 1.4 expected in a new production regime (Laws, 1991).

222 After the 7 February and the 15 March 2022, there was a strengthening of wind speeds, the XLD became deeper
223 than the MLD, probably entraining waters rich in DIC from the subsurface layer. Indeed, the CARIOCA measured
224 higher concentrations of DIC at the same time as higher wind speeds, and lower concentrations of $O_2 - O_{2sat}$ and of
225 Chl-a (Fig. 2 and Fig. 4). This might suggest that mixing events driven by high winds sometimes compensated for
226 the CO_2 undersaturation driven by biological activity. However, the mixing events shown here are only on synoptic
227 time scales. For instance, after the 10 February 2022, the wind decreased again and DIC concentrations stopped
228 increasing (Fig. 4 (a)). Overall, the CARIOCA measured low fCO_2 and DIC concentrations coinciding with high
229 concentrations of Chl-a and oxygen, during the whole summer 2022. This suggests that biological activity was the
230 dominant driver of the DIC seasonal variation, but the overall DIC concentration might have been even lower
231 without wind driven mixing.

232 3.3 Origin of fresh water mass and phytoplankton bloom

233 In summer 2022, the CARIOCA and glider were found in productive waters of low salinity (Fig. 2 and 3). The
234 presence of this low salinity upper ocean was also confirmed by the *S.A Agulhas II* thermosalinograph SSS
235 observations. Moreover, SSS images from the SMOS satellite mission, as well as salinity estimates, at 5 m, from
236 an ocean analysis (Mercator) and reanalysis (Glorys), and from an observational based gridded ocean salinity
237 estimate (ISAS), are all in agreement with the in-situ measurements and show low salinities in that region, in
238 summer 2022 (Fig. B2 in Appendix B). This surface fresh layer suggests a stratification of water masses, which
239 might have favoured the sustained growth of phytoplankton in a shallow mixed layer, where more light was
240 available.

241 To investigate the origin of these waters, we computed backward trajectories of virtual particles that were released
242 at the CARIOCA location. These particles were advected backward in a suite of different velocity field estimates,
243 at 15 m depth (see Methods). According to salinity maps from Mercator/Glorys, and to backward trajectories
244 spanning several months before the 2022 deployment of the instruments, the fresh water mass in which the
245 CARIOCA drifted was advected from a region south-west of their position, in the Weddell Sea. The formation of
246 this fresh water mass can be seen, from September to December 2021, using salinity maps and sea ice data from
247 OSI SAF (Fig. C1 in Appendix). The decrease in salinity started near the South Sandwich trench, around $25^\circ W$
248 and $60^\circ S$, near the sea ice edge in September 2021, when the sea ice started to retreat. It continued to develop
249 eastward near the sea ice edge until November 2021 (Fig. C1 in Appendix). Fig. 5 (b) shows the sea ice retreat
250 that month and the decrease in salinity that is very likely due to ice melt. The water mass then travelled north-east
251 (Fig. C1 and Fig. E1 in Appendix). In March 2022, the waters reaching CARIOCA still originated from the south-
252 west but then passed near Bouvet Island, before reaching the CARIOCA (Fig. E1 in Appendix). This corresponds
253 to a decrease in fCO_2 , DIC and increase in Chl-a (Fig. 2).



254

255 **Figure 5: (a) CCI Chl-a in November 2021, with sea ice mask (b) Mercator salinity change at 5 m in November 2021**
256 **(difference between the 30 November and 1 November), with black lines representing the sea ice concentration at 10%,**
257 **on the 1 November 2021 and on the 30 November 2021. Bottom figures represent a zoom of the region, with backward**
258 **trajectories (using Mercator, OSCAR and GlobCurrent total currents at 15 m depth) from the 7 February 2022 (from**
259 **CARIOCA's location) to the 1 November 2021.**

260 On Fig. 5, backward trajectories, computed using currents from OSCAR, Mercator / Glorys and GlobCurrent,
261 show that waters found at CARIOCA location (0.8° E, 54° S) on the 7 February 2022, came from a large
262 phytoplankton bloom (high Chl-a) that occurred in a region where surface salinity decreased at around 4-5 °W and
263 55.5-56.5 °S, near the sea ice edge, on the 1 November 2021. This corresponds to an export of waters from the
264 Weddell Sea, south of 55° S (Vernet et al., 2019). No satellite Chl-a data is available in October 2021 due to
265 clouds; however we can suppose that there was less sunlight available in October and that the phytoplankton bloom
266 formed in November 2021.

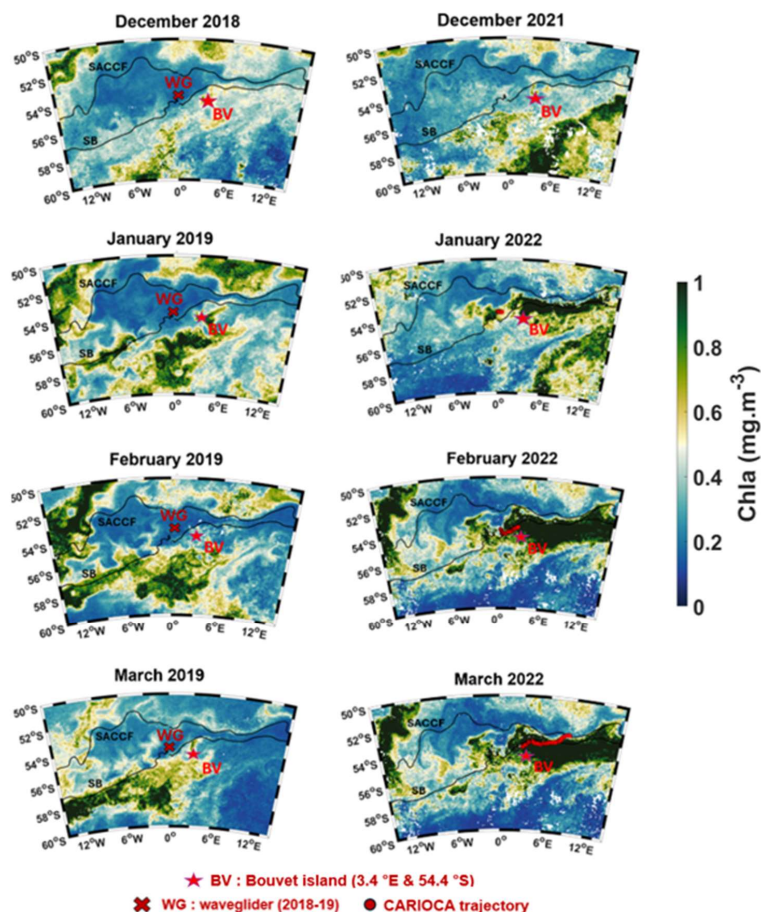
267 3.4 Comparison between spring-summer 2021-2022 and 2018-2019

268 Previous campaigns were conducted at the same season, near 54°S-0°W, in 2019 (Nicholson et al., 2022; Ogundare
269 et al., 2021). A comparison was therefore made between the summers 2022 and 2019. On 19 December 2018, a
270 Wave Glider (a surface autonomous vehicle) was deployed, at 0° E, 54° S (Nicholson et al., 2022). It stayed fixed
271 at this position for about two months, and performed surface measurements, until 11 February 2019. A comparison
272 was made between this Wave Glider and the CARIOCA surface data. The CARIOCA stayed near 0° E, 54° S,
273 from 26 January to 1 February 2022.

274 In 2019, the fCO₂ measured by the Wave Glider was near equilibrium with the atmosphere (2019 Wave Glider
275 fCO₂ ~ 410 µatm) whereas the CARIOCA buoy measured a large CO₂ undersaturation (2022 CARIOCA fCO₂ ~
276 330 µatm, Fig. 2a). In summer 2022 (from 26 January to 11 February 2022) the MLD was around 60 m, whereas
277 in summer 2019 (from 19 December 2018 to 11 February 2019) the MLD was deeper, around 100 m (not shown).
278 According to Nicholson's study, in 2019 the DIC concentration was around 2180 µmol kg⁻¹, while in January to



279 March 2022 it was much lower ($\sim 2130 \mu\text{mol kg}^{-1}$). After March, as the buoy went out of the Chl-a rich waters,
280 the CARIOCA DIC increased gradually, until it reached concentrations around $2170 \mu\text{mol kg}^{-1}$ in June 2022 (Fig.
281 2 (b)), close to the ones measured by the Wave Glider in 2019.

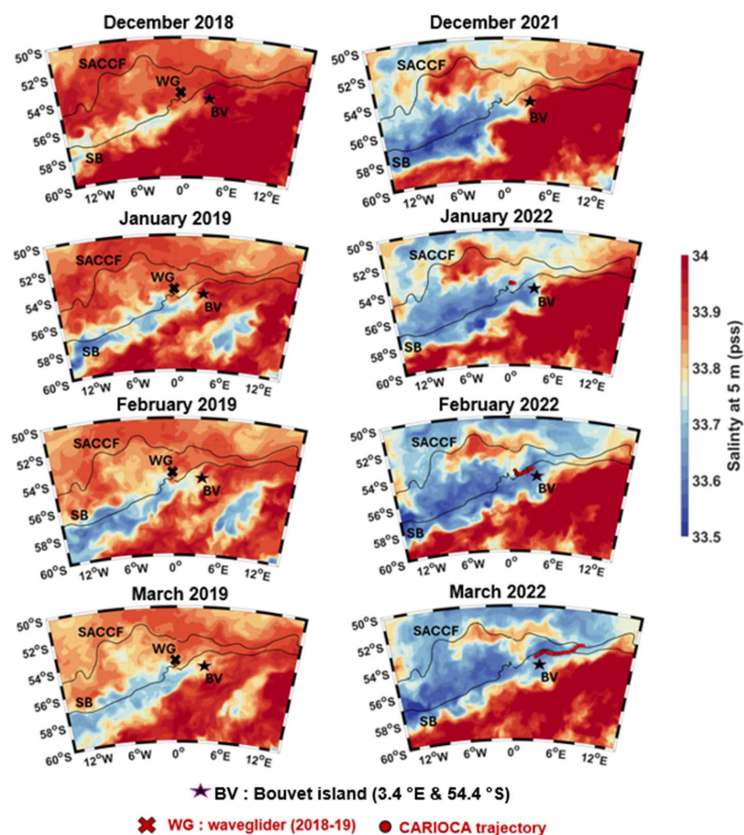


282
283 **Figure 6:** CCI Chl-a maps from December to March, left panel: 2018-2019, with waveglider position for the given month
284 in red, right panel: same as left, but for 2021-2022, with CARIOCA position for the given month in red. (SB: Southern
285 Boundary, SACCF: Southern Antarctic Circumpolar Current Front).

286 For the Chl-a comparison, CCI data were used to determine the Chl-a concentrations in the region in summer 2019
287 and 2022 (Fig. 6). From January to March 2022, a large phytoplankton bloom was observed around the Southern
288 Boundary, near the CARIOCA position (Fig. 6 (b)). This phytoplankton bloom was not present at the Wave Glider
289 and CARIOCA locations, in summer 2019 (Fig. 6 (a)). Indeed, around 0° E , 54° S , in 2019, there was no
290 chlorophyll-a. So, for different years, at the same position and for the same period, both instruments sampled
291 similar water masses but there was a large CO_2 undersaturation in summer 2022 not present in 2019. This is then
292 likely to be related to the large phytoplankton bloom present, at CARIOCA location, in January 2022. The
293 phytoplankton was farther south in January-March 2019. Indeed, in 2019, the phytoplankton stayed south of the
294 Southern Boundary (SB). The Chl-a concentrations were also lower in summer 2019 compared to 2022, and



295 reached up to 1.5 mg m^{-3} in 2022, whereas in 2019, the maximum Chl-a concentrations did not exceed 1 mg m^{-3} .
 296 In contrast, in January 2022, the CARIOCA entered in a phytoplankton bloom at 0° E , 54° S . The buoy then
 297 continued to sample waters rich in Chl-a in February and March 2022.



298
 299 **Figure 7: Mercator / Glorgys salinity at 5 m, from December to March, left panel: 2018-2019, with waveglider position**
 300 **for the given month in red, right panel: 2021-2022, with CARIOCA position for the given month in red. (SB: Southern**
 301 **Boundary, SACCF: Subantarctic Circumpolar Current Front).**

302 The phytoplankton bloom in summer 2022 in fact coincides with the presence of a fresh water mass. Mercator
 303 salinity profiles for spring 2021-summer 2022, show that this lower salinity was only present in the first 60 m,
 304 which also corresponds to the glider salinity profile. According to Mercator, in 2019, the lower salinities were
 305 much farther south (Fig. 7).

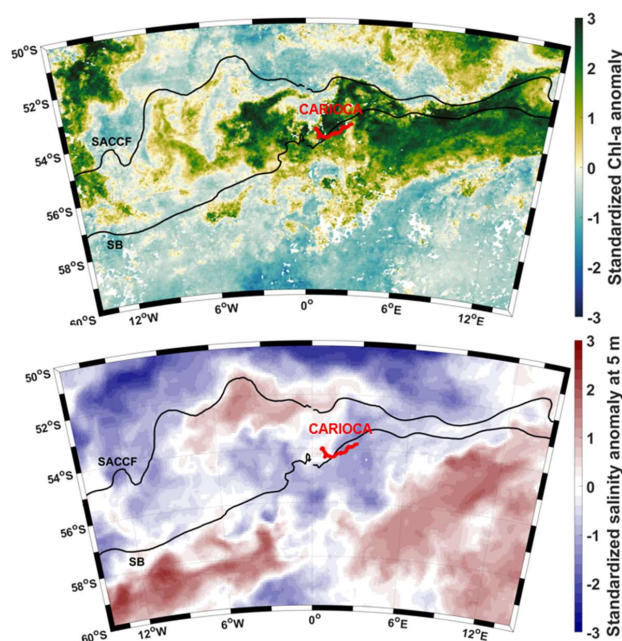
306 A comparison was also performed with surface transects of the Norwegian RV *Kronpins Haakon* cruise from the
 307 28 February 2019 to the 10 April 2019, (Ogundare et al., 2021). A ship transect crossed the CARIOCA path at
 308 around the same dates (end of March/beginning of April for both), for different years (2019 and 2022). North of
 309 the Southern Antarctic Circumpolar Current Front (SACCF), in April, the DIC, SST and SSS values for both years
 310 were consistent with each other. South of the SACCF, in 2019 the DIC concentration was higher ($\sim 2150 \mu\text{mol}$
 311 kg^{-1}) compared to the CARIOCA DIC concentration in 2022 (as low as $2120 \mu\text{mol kg}^{-1}$, South of the SACCF).
 312 The ship's path in 2019, south of the SACCF, was between $5\text{-}8^\circ \text{ E}$ and $53\text{-}57^\circ \text{ S}$, where the Chl-a concentrations



313 were low (Fig. 6). At these positions, higher salinities and temperatures were also measured by the RV *Kronpins*
314 *Haakon*, in 2019 (SSS ~ 34 pss before April 2019) (Fig. D1 in Appendix).

315 4. Discussion

316 In summer 2022, the CARIOCA buoy crossed a massive phytoplankton bloom (Figure 1) and measured an
317 unusually large CO₂ sink near the Southern Boundary and Bouvet Island, east of 0° E, 54° S (Figure 2a). According
318 to pCO₂ climatologies (Takahashi et al., 2012) or recent in situ measurements in 2019 (Nicholson et al., 2022;
319 Ogundare et al., 2021), this region is usually in equilibrium with the atmosphere or is a much smaller carbon sink
320 than the one observed in summer 2022. Sergi et al. (2020) showed that moderate bloom can develop around Bouvet
321 Island by a combination of fertilization from the island itself and from the proximity of seamounts acting as
322 hydrothermal sources of iron. However, the bloom observed in summer 2022 (Fig. 1b) was more massive. In fact,
323 it was the largest bloom observed over the past twelve years (Fig. 8a) (and also over the last 25 years, not shown),
324 as large as those typically observed on the Kerguelen Plateau (Blain et al., 2007).



325
326 **Figure 8: Anomalies in February 2022, relative to a 2011–2022 climatology, normalised with the standard deviation of**
327 **monthly values for: (a) Chl-a and (b) Salinity at 5 m using Mercator analysis. CARIOCA trajectory in February (red).**

328 Moreover, the Lagrangian backward trajectories for the January–February 2022 bloom are not consistent with an
329 origin from Bouvet Island or from seamounts, in contrast with the case in Sergi et al. (2020). Another possible
330 source of iron fertilization could come from the melting of icebergs (Person et al., 2019). An analysis of satellite
331 images enables us to rule out the hypothesis of iceberg melting in the vicinity of the CARIOCA drifter, or of water
332 fertilised by the melting of the supergiant iceberg A68A (Smith and Bigg, 2023) that happened near South Georgia
333 in Fall 2021, being the cause of the bloom. Although there were some iceberg fragments present near the
334 CARIOCA after its deployment, in January 2022 (Fig. S2 in Supplement), the large size of the fresh water mass



335 coming from the south-east, all point towards an export of fresh waters from the Weddell Sea. Salinity was
336 anomalously fresh (Fig 8b), although there was no significant rainfall during that period at the position of the fresh
337 water mass (not shown). Both salinity maps (from Mercator/Glorys) and backward trajectories enable us to track
338 the travel of this fresh water mass, from its formation in spring 2021, to the position of the CARIOCA and glider,
339 in summer 2022. The fresh water mass was formed near the sea ice edge (from September 2021 to November
340 2021, Fig. C1). Indeed, in 2021, the ice retreated abnormally early, from September to mid-November 2021,
341 anomalous north-eastward motion of sea ice was observed in the north-east Weddell Sea (Wang et al., 2022, their
342 Fig. 3 and 4) and the austral summer 2022 marked a record for the lowest sea ice extent in Antarctica (Wang et
343 al., 2022).

344 **4.1 Impact of anomalous sea ice retreat on phytoplankton blooms**

345 Previous studies have shown that the melting of sea ice can fertilise the region near the sea ice edge and stratify
346 the water masses (Briggs et al., 2018; McClish and Bushinsky, 2023). We can suppose that this is what promoted
347 the development of a phytoplankton bloom at the sea ice edge in spring 2021 (Fig. 5a). Model results of Death et
348 al. (2014) also suggested that subglacial meltwaters may constitute a significant additional source of bioavailable
349 iron to the Southern Ocean, supplementing iceberg sources, and that the impact of the glacial iron flux may be
350 large, extending across much of the Southern Ocean due to the redistribution of the iron by ocean circulation.

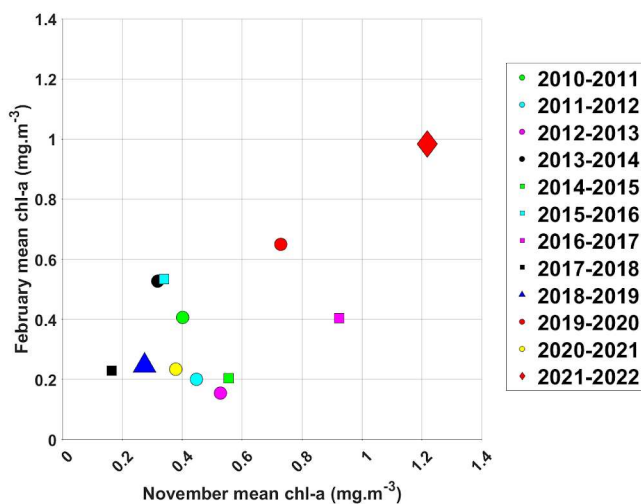
351 We can thus infer that phytoplankton bloom near CARIOCA trajectory in January-February 2022 was favoured
352 by stratified, fresher waters (Fig. 8b) and micro nutrients supplied by ice melt and redistributed by ocean
353 circulation. This is supported by fresh and enriched Chl-a water that detached from the sea ice edge region around
354 4°W in November 2021 and migrated north-westward (Fig. 5). This leads to the presence, in December 2021, of
355 a patch of moderate Chl-a around 6°W 57°S (Fig. 6) along the Lagrangian backward trajectory (Fig. E1 in
356 Appendix). Then, this patch migrates north-eastward, and reaches the CARIOCA in January 2022, with Chl-a
357 slightly higher than in December, possibly because of additional fertilization by nearby seamounts or because of
358 the presence of different phytoplankton community composition. In March 2022, the waters reaching CARIOCA
359 originated from farther south, closer to the ice (Fig. E1 in Appendix), then passed near Bouvet Island, before
360 reaching the CARIOCA (Fig. E1). Hence these waters might have been even more enriched in micro nutrients
361 related to sea ice melt. Also, as shown by previous studies, the proximity of Bouvet Island might have further
362 fertilised the region (Sergi et al., 2020). This is consistent with the decrease in DIC and increase in Chl-a observed
363 by CARIOCA from the beginning of March (Fig. 2).

364

365 **4.2 Interannual variation**

366 The backward trajectories show that waters near 0°S, 54°S in February, generally came from the south-west the
367 previous years as well (Fig. S4). We therefore investigate a possible link between the intensity of the bloom at the
368 extremities of the Lagrangian backward trajectory between November and February, from 2010 to 2022, to study
369 a possible link between spring blooms near the sea ice edge and summer blooms near Bouvet Island.

370 In spring 2021-summer 2022, the blooms at both extremities of the backward trajectories were much more
371 pronounced than usual, with Chl-a concentrations above 1 mg.m⁻³ in both November 2021 (along the backward
372 trajectory) and in February 2022 (along the CARIOCA trajectory) (Figure 9).



373

374 **Figure 9: Mean Chl-a along CARIOCA position in February plotted against the mean Chl-a along the backward**
375 **trajectories (computed using OSCAR currents) in November, for each year from 2010 to 2022.**

376 This supports the hypothesis that there might be a link between the fertilization near the sea ice edge and the
377 biological activity at the CARIOCA location. This also suggests that a strong spring bloom, promoted by sea ice
378 retreat, could promote the development of a strong summer bloom farther north. Following the same logic, when
379 low concentrations of Chl-a were observed in November, similarly low concentrations of Chl-a were usually
380 observed in February (see for instance 2018-2019, Fig. 9).

381 **4.3 Interpretation of the low DIC and fCO₂ observed by CARIOCA**

382 During sea ice retreat, large net community production occurs in the seasonal ice zone (SIZ), likely due to iron
383 delivery or low grazing rates (McClish and Bushinsky, 2023). Moreover, these authors found, based on BGC Argo
384 floats observations, that the bloom NCP increases in case of early sea ice retreat. Given that the water mass
385 reaching the CARIOCA subpolar region remained in the bloom near sea ice edge from September to November
386 2021, i.e. over the whole bloom period, it seems reasonable to consider that the DIC of this water mass was affected
387 by a bloom NCP typical of early ice retreat, of 3 molC m⁻² (Figure 4 of McClish and Bushinsky, 2023) which
388 would correspond to a fCO₂ as low as 240 μatm (Appendix F). Assuming that from end November 2021 to January
389 2022, the fCO₂ change along the water mass trajectory was only affected by air-sea exchange and temperature
390 change, we estimate a fCO₂ of 342 μatm at the end of January 2022 (see details in Appendix F), a value very close
391 to the one observed by CARIOCA (Figure 2a). In this crude estimation, we neglect biological production along
392 the water mass trajectory and mixing with subsurface water. The latter seems at first order reasonable given that
393 the salinity anomaly persisted along the water mass trajectory until January 2022. For what concerns the biological
394 activity, the Chl-a was much lower along the water mass trajectory in December 2021-January 2022 than in the
395 vicinity of the sea ice edge in spring 2021, suggesting low NCP. Moreover, the DIC derived from CARIOCA
396 observations in January-February 2022 remained relatively stable suggesting a balance between biological
397 production and other processes, such as subsurface mixing or consumption by grazers.



398 **4.4 Study limits and perspectives**

399 Our Chl-a study was focused only on the region surrounding Bouvet Island, from 50° S to 60° S, and 15° W to
400 15° E. We could envision further studies on the impact of sea ice retreat at latitudes farther north, in the whole
401 Southern Ocean, not just in the Atlantic sector. The kind of analysis performed in this study could be extended on
402 other islands in the Southern Ocean and see if the combined effect of sea ice retreat and fertilization from the
403 island, could enhance phytoplankton development around other Southern Ocean islands. The year 2022 was a
404 record for lowest sea ice extent in austral summer (Wang et al., 2022). We could hypothesise that the productive
405 waters travelled farther north than usual, due to this unprecedented low sea ice extent record. It has been shown
406 that due to global warming, there is a tendency for more sea ice retreat in the Southern Ocean in the future (Wang
407 et al., 2022). This could lead to stronger undersaturation of $f\text{CO}_2$ in regions usually in equilibrium with the
408 atmosphere in austral summer. Phytoplankton travelling to higher “northern” latitudes could also lead to a shift in
409 the hunting zones of predators and might therefore have an impact on the ecosystem, in the long term. Studies
410 have shown that due to higher emissions and a warmer climate, there might be a change in the future location,
411 mechanism and seasonality of the carbon sink in the Southern Ocean, with an increase of CO_2 uptake in certain
412 regions (Hauck et al., 2015; Mongwe et al., 2024). In this context, events such as the one observed in summer
413 2022, that is, an increased sea ice retreat leading to a shift of the CO_2 sink to higher “northern” latitudes, should
414 become more frequent, and should be monitored carefully.

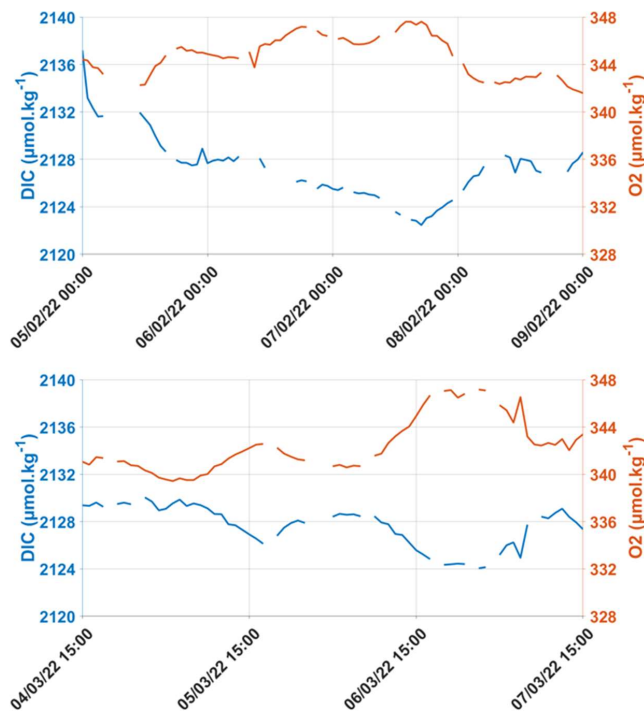
415 **5. Conclusion**

416 Lagrangian backward trajectories suggest that the summer 2022 phytoplankton bloom in the subpolar ocean is
417 mainly due to early sea ice retreat the previous spring and not due to the proximity of Bouvet Island or seamounts,
418 as was the case in Sergi et al. (2020). Although there was probably some contribution, in March 2022, due to
419 fertilization from Bouvet Island, the CARIOCA buoy was already in Chl-a rich waters, at the end of January 2022,
420 west of Bouvet. Indeed, the phytoplankton bloom in which the CARIOCA entered did not originate from Bouvet
421 Island but coincides with the presence of a fresh water mass. Mercator/Glorys salinity maps and Lagrangian
422 backward trajectories, from November 2021 to March 2022, show that this fresh water mass sampled by the buoy
423 and the glider, originate from the vicinity of sea ice edge, south-west of the instruments’ deployment, at around 4-
424 5° W and 55.5-56.5° S. Early sea ice retreat in spring 2021 fuelled seawater with micro nutrients leading to a large
425 phytoplankton bloom near sea ice edge, which then travelled to the CARIOCA position. These waters were likely
426 already depleted in carbon near sea ice edge when they escaped towards CARIOCA location which led to very
427 undersaturated CARIOCA $f\text{CO}_2$. This shows that productive waters from the sea ice edge travelled farther north
428 than usual, up to 54° S, causing a strong undersaturation of $f\text{CO}_2$ in regions usually known to be in equilibrium
429 with the atmosphere. Austral summer 2022 was a record for an unusually low sea ice extent (Wang et al., 2022).
430 Our observations highlight the northward migration of the CO_2 sink associated with early sea ice retreat, a
431 phenomenon projected by Earth System Models under climate change (Mongwe et al. 2024), with significant
432 reduction in biologically-derived $f\text{CO}_2$ associated with melting ice, and the consequent increase in the oceanic CO_2
433 sink in certain sectors of the Southern Ocean.



434 **Appendix**

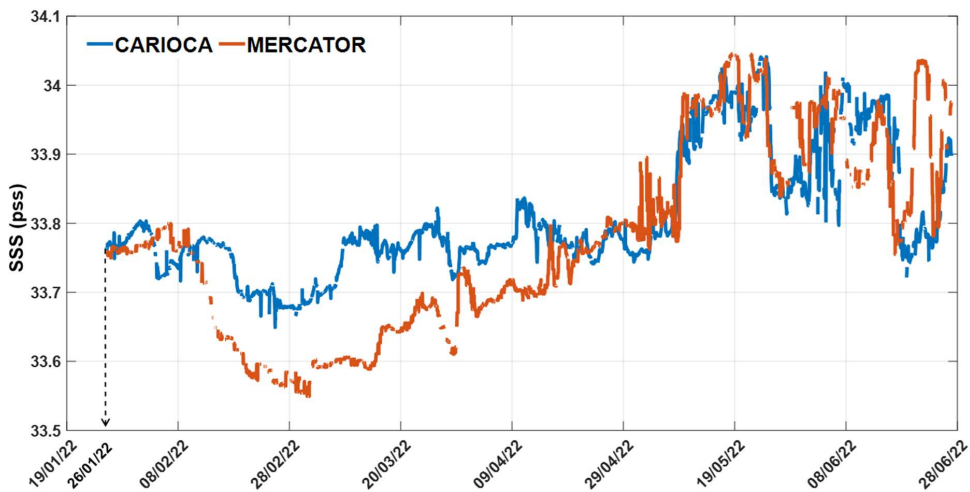
435 **Appendix A: Net Community Production (NCP) estimations**



436

437 **Figure A1: DIC and O₂ (uncorrected) for periods during which NCP was estimated, in summer 2022.**

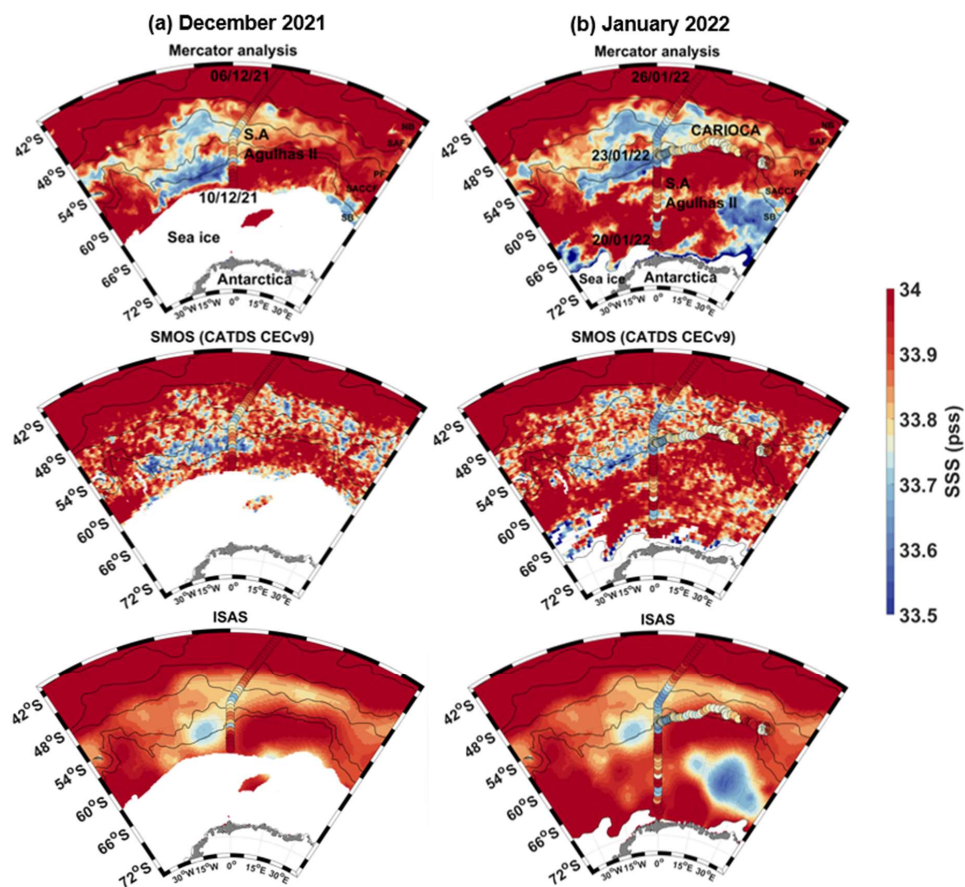
438 **Appendix B: Comparison between salinity products and CARIOCA SSS**



439

440 **Figure B1: Colocalization between CARIOCA hourly SSS, at 2 m, and Mercator's daily salinity, at 5 m, from the 26**

441 **January to the 27 June 2022.**



442

443

444

445

446

447

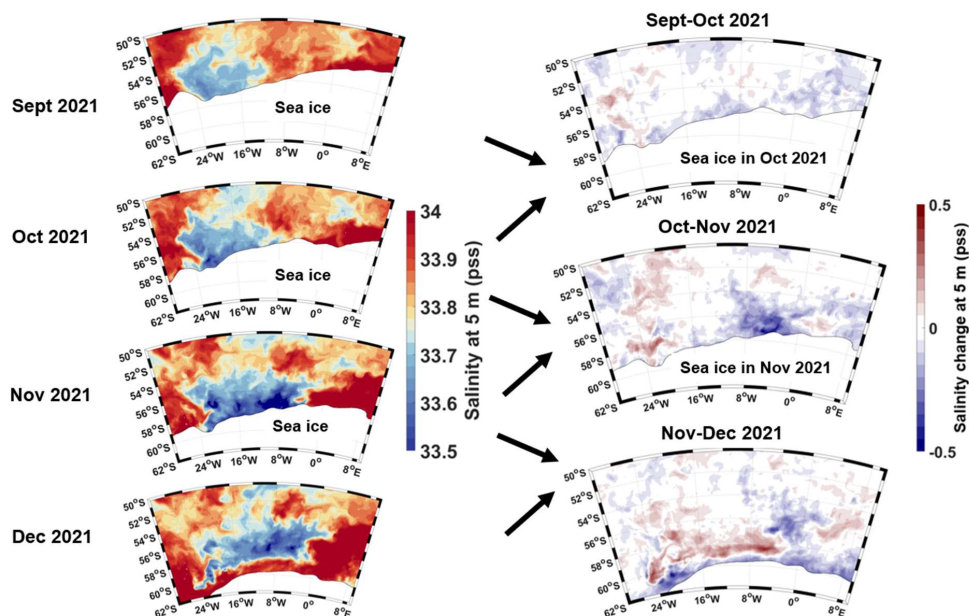
448

Figure B2: Mercator salinity at 5 m, SMOS CATDS CECv9.0 SSS, and ISAS (MY) salinity at 5 m, with sea ice mask (0 % threshold of sea ice concentration) and fronts superimposed, (a) December 2021 mean SSS map, with *S.A. Agulhas II* SSS from the 6-10 December 2021, (b) January 2022 mean SSS map, with *CARIOCA* SSS from the 26 January 2022 to the 27 June 2022, and *S.A. Agulhas II* SSS from the 20-26 January 2022. SMOS SSS was adjusted by -0.1 pss to fit with *CARIOCA* and *S.A. Agulhas II* SSS.

448



449 **Appendix C: Origin of fresh water mass**



450

451 **Figure C1: (a) Mercator salinity at 5 m, with sea ice (10 % threshold of sea ice concentration, from OSI SAF) receding**
452 **from September to December 2021, (b) corresponding salinity change maps.**

453

454

455

456

457

458

459

460

461

462

463

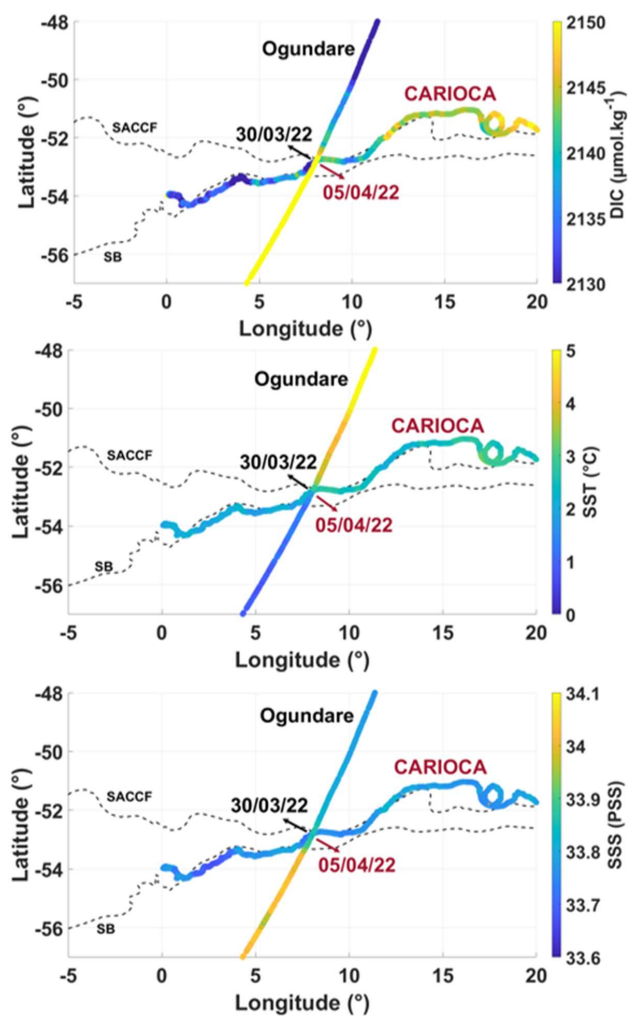
464

465

466



467 **Appendix D: Comparison between summers 2022 and 2019**

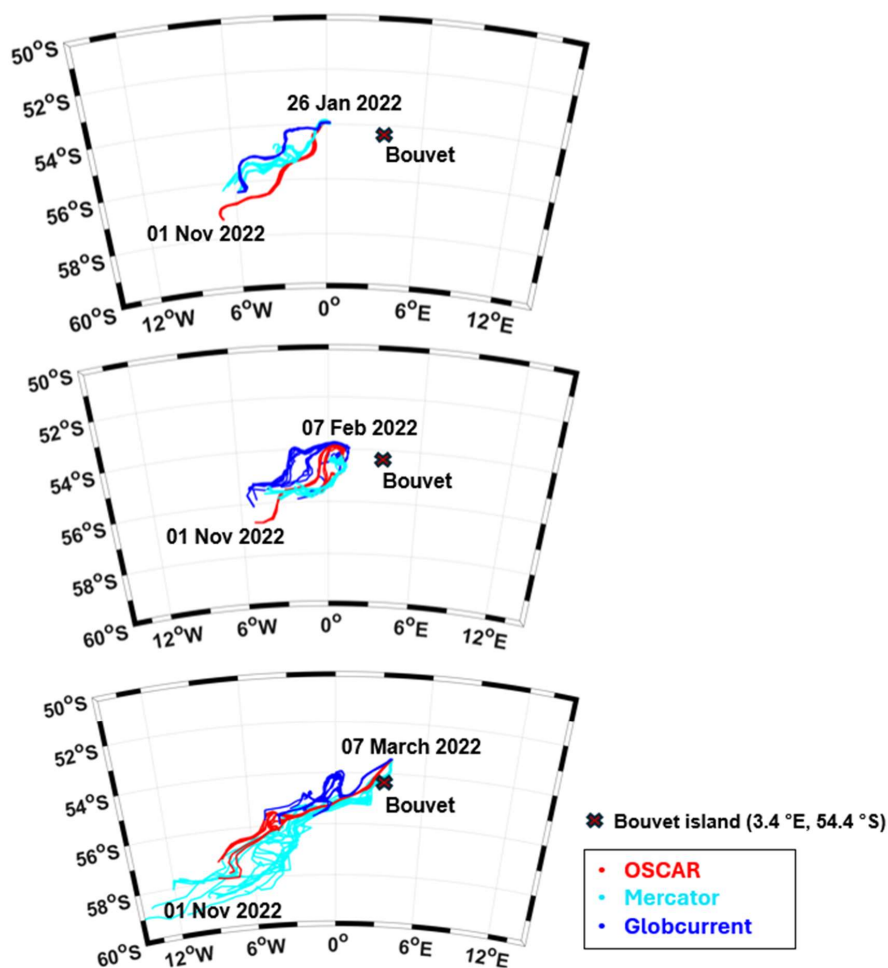


468

469 **Figure D1: DIC, SST and SSS of CARIOCA SO-CHIC (2022) and Ogundare (2019).**



470 **Appendix E: Origin of summer 2022 phytoplankton bloom**



471

472 **Figure E1: Backward trajectories from January, February, and March 2022 to November 2021, using different current**
473 **products (Mercator analysis, OSCAR, Globcurrent).**

474

475

476

477

478



479 **Appendix F: Estimation of DIC and fCO₂ variations along the water mass trajectory**

480 Neglecting mixing and neglecting dfCO₂ due to salinity change,
481 the monthly changes of fCO₂ are estimated as in Merlivat et al. (2015):

$$482 \Delta fCO_2 = \Delta fCO_{2SST} + (\delta fCO_2 / \delta DIC) \Delta DIC \quad (F1)$$

483 *With*

$$484 dfCO_2 / dt = (\partial fCO_2 / \partial T) dT / dt + (\partial fCO_2 / \partial DIC) dDIC / dt \quad (F2)$$

$$485 \partial fCO_2 / \partial T = (0.0423 \text{ } ^\circ\text{C}^{-1}) fCO_2 \quad (F3)$$

$$486 \partial fCO_2 / \partial DIC = R(fCO_2 / DIC), \text{ where } R \text{ is the Revelle factor} \quad (F4)$$

$$487 \text{Neglecting mixing: } \Delta DIC = \Delta DIC_{(bio)} + \Delta DIC_{(air-sea)} \quad (F5)$$

488 Where $\Delta DIC_{(bio)}$ is the contribution from biological production, and $\Delta DIC_{(air-sea)}$ is the contribution from the air-sea flux.

$$490 \Delta DIC_{(air-sea)} = F / (\rho * MLD), \text{ where } \rho \text{ is the seawater density and } F \text{ is the air-sea flux (Eq.(1))} \quad (F6)$$

491 We assume an exchange coefficient, K, of 0.1/12 mol m⁻² month⁻¹ μatm^{-1} (Boutin et al., 2009), and a Revelle factor, R, of 16 (Sabine et al., 2004).

493 According to (McClish and Bushinsky, 2023) the highest rates of daily net community production occur during active sea ice retreat and the bloom net community production is higher in case of early sea ice retreat. Given that the water mass reaching the CARIOCA subpolar region remained in the bloom near sea ice edge from September to November 2021, i.e. over the whole bloom period, it seems reasonable to consider that the DIC of this water mass was affected by a bloom NCP typical of early ice retreat, of 3 molC m⁻² bloom⁻¹ (Figure 4 of McClish and Bushinsky, 2023). The MLD measured by the glider in summer 2022 is around 60 m. Assuming the same MLD depth in spring 2021, we estimate that the $\Delta DIC_{(bio)}$ due to the bloom near sea ice edge in spring 2021 was -50 $\mu\text{mol kg}^{-1}$. Assuming a DIC concentration before melting around 2200 $\mu\text{mol kg}^{-1}$ (Briggs et al., 2018) and fCO₂ initially in equilibrium with the atmosphere (fCO₂ ~ 400 μatm), the decrease in fCO₂ in November due to bloom NCP is estimated to be -160 μatm (November fCO₂ ~ 240 μatm).

503 We then assume that, at first order, the fCO₂ change along the water mass trajectory is only affected by air-sea exchange and temperature change (i.e. we neglect biological production along the water mass trajectory and mixing with subsurface water, which seems at first order reasonable given the relatively low Chl-a along the water mass trajectory than in the vicinity of the sea ice edge, and given that the salinity anomaly persisted along the water mass trajectory until January 2022 respectively).

508 *From November 2021 to December 2021*, $\Delta DIC_{(air-sea)} = 22 \mu\text{mol kg}^{-1}$ and the $\partial fCO_{2(air-sea)}$ is +42 μatm . After the air-sea flux correction, we obtain a DIC concentration of about 2172 $\mu\text{mol kg}^{-1}$, and an fCO₂ of 282 μatm . The waters from sea ice melt are at -1.8 °C (seawater's freezing point). According to Remote Sensing System (REMSS, C.f. Data sets) and to backward trajectories, the SST along the water mass trajectory was -0.5 °C at the end of November 2021. Considering a heating of 1.3 °C ($\partial T = +1.3 \text{ } ^\circ\text{C}$) during the month of November, the temperature effect leads to an increase in fCO₂ of +15 μatm . At the end of December 2021, the fCO₂ is therefore 297 μatm .

514 *In January 2022*, $\Delta DIC_{(air-sea)}$ is +14 $\mu\text{mol kg}^{-1}$, and the $\partial fCO_{2(air-sea)}$ is +31 μatm . After the air-sea flux correction the fCO₂ is 328 μatm and the DIC is 2186 $\mu\text{mol kg}^{-1}$. According to REMSS and to backward trajectories, ∂T is +1.0 °C, the $\partial fCO_{2(SST)}$ is 14 μatm . At the end of January 2021, the fCO₂ estimate is therefore 342 μatm .



517 **Data Availability**

518 All data used in this study are freely available and downloadable from the following websites. CARIOCA dataset
519 is available on SEANOE at <https://doi.org/10.17882/100800>. The Seaglider (675) dataset is available online at
520 <https://doi.org/10.5281/zenodo.11059426>. The *S.A. Agulhas II* SO-CHIC 2022 cruise TSG dataset is available
521 on SEANOE at <https://doi.org/10.17882/100905>. The *S.A. Agulhas II* SO-CHIC 2022 cruise, CTD data is available
522 on SEANOE at <https://doi.org/10.17882/95314>. ERA5 atmospheric pressure and wind speed hourly data on single
523 levels from 1940 to present is available on Copernicus Climate Change Service Climate Data Store , at
524 <https://doi.org/10.24381/cds.adbb2d47>. The « Global Ocean Physics Reanalysis » and the « Global Ocean Physics
525 Analysis and Forecast » datasets are available on Copernicus Marine at <https://doi.org/10.48670/moi-00021> and
526 <https://doi.org/10.48670/moi-00016>. The SMOS CATDS CECv9 salinity dataset is available online at
527 <https://doi.org/10.17882/52804#102161>. The ISAS MultiYear salinity dataset is available on the data store of
528 Copernicus Marine, at <https://doi.org/10.17882/46219>. The OSCAR dataset is available at
529 <https://doi.org/10.5067/OSCAR-03D01>. The Globcurrent dataset is available at <https://doi.org/10.48670/mds-00327>.
530 The OCI-CCI chlorophyll-a dataset is available online at <http://www.oceancolour.org>. The MW OI SST
531 dataset produced by Remote Sensing Systems is available online at www.remss.com. The datasets “Global Sea
532 Ice Concentration Climate Data Record v3.0 - Multimission, EUMETSAT SAF on Ocean and Sea Ice” and
533 “Global Sea Ice Concentration Interim Climate Data Record Release 3 - DMSP, EUMETSAT SAF on Ocean and
534 Sea Ice” are available online at http://doi.org/10.15770/EUM_SAF_OSI_0013 and
535 http://doi.org/10.15770/EUM_SAF_OSI_0014. The SPASSO package containing the LAMTA software used for
536 the lagrangian analysis can be downloaded at <https://www.swot-adac.org/resources/spasso/>

537 **Supplement**

538 The supplement related to this article is joined as a separate file to this submission.

539 **Author contributions**

540 J.Boutin oversaw the study, helped in the data processing, in the estimations, in the analysis and interpretation of
541 the results and in the conception of the paper. S.Swart and M.du Plessis provided the Seaglider (675) dataset. They
542 also provided useful input concerning the Seaglider data processing and interpretation of the results. L.Merlivat
543 provided useful inputs and insights during the progress of this study, suggesting various hypotheses and helping
544 us investigate them. L.Beaumont oversaw the verification of the calibration of CARIOCA sensors. A.Lourenco
545 helped in the deployment of the CARIOCA buoy during the SO-CHIC 2022 cruise. Their involvement during the
546 COVID period enabled us to collect data vital to this study. F.d’Ovidio and L.Rousselet provided the python code
547 used for the Lagrangian analysis, which is the basis of our study and without which we couldn’t have proved the
548 origin of the phytoplankton bloom. They helped with discussions and modifications related to this code, for our
549 specific study case. B.Ward provided the TSG data of the *S.A. Agulhas II* ship (SO-CHIC 2022). J.B.Sallée
550 coordinated the SO-CHIC project, and provided part of the financial support. All co-authors discussed, reviewed,
551 and edited the paper.



552 **Competing interests**

553 The contact author has declared that none of the authors has any competing interests.

554 **Acknowledgements**

555 The authors would like to thank Dimitry Khvorostyanov (dimitry.khvorostyanov@locean.ipsl.fr) and Alain
556 Laupin-Vinatier (alain.laupin-vinatier@locean.ipsl.fr) for the automation of CARIOCA data processing chain in
557 real time. We also thank S.Nicholson and M.Vancoppenolle for helpful discussions.

558 **Financial support**

559 This project has been partly funded by the SO-CHIC programme. L. Rousselet is supported by the CNES TOSCA
560 Bioswot-AdAC project.

561 **References**

562 Ardyna, M., Lacour, L., Sergi, S., d'Ovidio, F., Sallée, J.-B., Rembauville, M., Blain, S., Tagliabue, A., Schlitzer,
563 R., Jeandel, C., Arrigo, K. R., and Claustre, H.: Hydrothermal vents trigger massive phytoplankton blooms in the
564 Southern Ocean, *Nat. Commun.*, 10, 2451, <https://doi.org/10.1038/s41467-019-09973-6>, 2019.

565 Bakker, D. C. E., Pfeil, B., Landa, C. S., Metzl, N., O'Brien, K. M., Olsen, A., Smith, K., Cosca, C., Harasawa,
566 S., Jones, S. D., Nakaoka, S., Nojiri, Y., Schuster, U., Steinhoff, T., Sweeney, C., Takahashi, T., Tilbrook, B.,
567 Wada, C., Wanninkhof, R., Alin, S. R., Balestrini, C. F., Barbero, L., Bates, N. R., Bianchi, A. A., Bonou, F.,
568 Boutin, J., Bozec, Y., Burger, E. F., Cai, W.-J., Castle, R. D., Chen, L., Chierici, M., Currie, K., Evans, W.,
569 Featherstone, C., Feely, R. A., Fransson, A., Goyet, C., Greenwood, N., Gregor, L., Hankin, S., Hardman-
570 Mountford, N. J., Harlay, J., Hauck, J., Hoppema, M., Humphreys, M. P., Hunt, C. W., Huss, B., Ibáñez, J. S. P.,
571 Johannessen, T., Keeling, R., Kitidis, V., Körtzinger, A., Kozyr, A., Krasakopoulou, E., Kuwata, A., Landschützer,
572 P., Lauvset, S. K., Lefèvre, N., Lo Monaco, C., Manke, A., Mathis, J. T., Merlivat, L., Millero, F. J., Monteiro, P.
573 M. S., Munro, D. R., Murata, A., Newberger, T., Omar, A. M., Ono, T., Paterson, K., Pearce, D., Pierrot, D.,
574 Robbins, L. L., Saito, S., Salisbury, J., Schlitzer, R., Schneider, B., Schweitzer, R., Sieger, R., Skjelvan, I.,
575 Sullivan, K. F., Sutherland, S. C., Sutton, A. J., Tadokoro, K., Telszewski, M., Tuma, M., van Heuven, S. M. A.
576 C., Vandemark, D., Ward, B., Watson, A. J., and Xu, S.: A multi-decade record of high-quality CO₂ data in version
577 3 of the Surface Ocean CO₂ Atlas (SOCAT), *Earth Syst. Sci. Data*, 8, 383–413, [https://doi.org/10.5194/essd-8-](https://doi.org/10.5194/essd-8-383-2016)
578 383-2016, 2016.

579 Blain, S., Quéguiner, B., Armand, L., Belviso, S., Bombled, B., Bopp, L., Bowie, A., Brunet, C., Brussaard, C.,
580 Carlotti, F., Christaki, U., Corbière, A., Durand, I., Ebersbach, F., Fuda, J.-L., Garcia, N., Gerringa, L., Griffiths,
581 B., Guigue, C., Guillermin, C., Jacquet, S., Jeandel, C., Laan, P., Lefèvre, D., Lo Monaco, C., Malits, A., Mosseri,
582 J., Obernosterer, I., Park, Y.-H., Picheral, M., Pondaven, P., Remenyi, T., Sandroni, V., Sarthou, G., Savoye, N.,
583 Scouarnec, L., Souhaut, M., Thuiller, D., Timmermans, K., Trull, T., Uitz, J., van Beek, P., Veldhuis, M., Vincent,
584 D., Viollier, E., Vong, L., and Wagener, T.: Effect of natural iron fertilization on carbon sequestration in the
585 Southern Ocean, *Nature*, 446, 1070–1074, <https://doi.org/10.1038/nature05700>, 2007.

586 Boutin, J., Merlivat, L., HÉnocq, C., Martin, N., and Sallée, J. B.: Air-sea CO₂ flux variability in frontal regions
587 of the Southern Ocean from CARbon Interface OCEan Atmosphere drifters, *Limnol. Oceanogr.*, 53, 2062–2079,
588 https://doi.org/10.4319/lo.2008.53.5_part_2.2062, 2008.

589 Boutin, J., Quilfen, Y., Merlivat, L., and Piolle, J. F.: Global average of air-sea CO₂ transfer velocity from
590 QuikSCAT scatterometer wind speeds, *J. Geophys. Res. Oceans*, 114, <https://doi.org/10.1029/2007JC004168>,
591 2009.

592 Boutin, J., Vergely, J.-L., Khvorostyanov, D., and Supply, A.: SMOS SSS L3 maps generated by CATDS CEC
593 LOCEAN. debias V8.0, <https://doi.org/10.17882/52804>, 2023.



- 594 Briggs, E. M., Martz, T. R., Talley, L. D., Mazloff, M. R., and Johnson, K. S.: Physical and Biological Drivers of
595 Biogeochemical Tracers Within the Seasonal Sea Ice Zone of the Southern Ocean From Profiling Floats, *J.*
596 *Geophys. Res. Oceans*, 123, 746–758, <https://doi.org/10.1002/2017JC012846>, 2018.
- 597 Copin-Montégut, C., Bégovic, M., and Merlivat, L.: Variability of the partial pressure of CO₂ on diel to annual
598 time scales in the Northwestern Mediterranean Sea, *Mar. Chem.*, 85, 169–189,
599 <https://doi.org/10.1016/j.marchem.2003.10.005>, 2004.
- 600 C3S: ERA5 hourly data on single levels from 1940 to present, <https://doi.org/10.24381/CDS.ADBB2D47>, 2018.
- 601 de Boyer Montégut, C., Madec, G., Fischer, A. S., Lazar, A., and Iudicone, D.: Mixed layer depth over the global
602 ocean: An examination of profile data and a profile-based climatology, *J. Geophys. Res. Oceans*, 109,
603 <https://doi.org/10.1029/2004JC002378>, 2004.
- 604 Death, R., Wadham, J. L., Monteiro, F., Le Brocq, A. M., Tranter, M., Ridgwell, A., Dutkiewicz, S., and Raiswell,
605 R.: Antarctic ice sheet fertilises the Southern Ocean, *Biogeosciences*, 11, 2635–2643, [https://doi.org/10.5194/bg-](https://doi.org/10.5194/bg-11-2635-2014)
606 11-2635-2014, 2014.
- 607 DeVries, T.: The oceanic anthropogenic CO₂ sink: Storage, air-sea fluxes, and transports over the industrial era,
608 *Glob. Biogeochem. Cycles*, 28, 631–647, <https://doi.org/10.1002/2013GB004739>, 2014.
- 609 d’Ovidio, F., Della Penna, A., Trull, T.W., Nencioli, F., Pujol, M.-I., Rio, M.-H., Park, Y.-H., Cotté, C., Zhou, M.,
610 and Blain, S. (2015). The biogeochemical structuring role of horizontal stirring: Lagrangian perspectives on iron
611 delivery downstream of the Kerguelen plateau. *Biogeosciences* 12, 5567–5581.
- 612 EUMETSAT - Product Navigator - Global Sea Ice Concentration Climate Data Record v3.0 - Multimission:
613 <https://navigator.eumetsat.int/product/EO:EUM:DAT:0826>, last access: 10 July 2024.
- 614 EUMETSAT - Product Navigator - Global Sea Ice Concentration Interim Climate Data Record Release 3 -
615 DMSP: <https://navigator.eumetsat.int/product/EO:EUM:DAT:0645>, last access: 10 July 2024.
- 616 Friedlingstein, P., O’Sullivan, M., Jones, M. W., Andrew, R. M., Bakker, D. C. E., Hauck, J., Landschützer, P.,
617 Le Quéré, C., Luijkx, I. T., Peters, G. P., Peters, W., Pongratz, J., Schwingshackl, C., Sitch, S., Canadell, J. G.,
618 Ciais, P., Jackson, R. B., Alin, S. R., Anthony, P., Barbero, L., Bates, N. R., Becker, M., Bellouin, N., Decharme,
619 B., Bopp, L., Brasika, I. B. M., Cadule, P., Chamberlain, M. A., Chandra, N., Chau, T.-T.-T., Chevallier, F., Chini,
620 L. P., Cronin, M., Dou, X., Enyo, K., Evans, W., Falk, S., Feely, R. A., Feng, L., Ford, D. J., Gasser, T., Ghattas,
621 J., Gkritzalis, T., Grassi, G., Gregor, L., Gruber, N., Gürses, Ö., Harris, I., Hefner, M., Heinke, J., Houghton, R.
622 A., Hurtt, G. C., Iida, Y., Ilyina, T., Jacobson, A. R., Jain, A., Jarníková, T., Jersild, A., Jiang, F., Jin, Z., Joos, F.,
623 Kato, E., Keeling, R. F., Kennedy, D., Klein Goldewijk, K., Knauer, J., Korsbakken, J. I., Körtzinger, A., Lan, X.,
624 Lefèvre, N., Li, H., Liu, J., Liu, Z., Ma, L., Marland, G., Mayot, N., McGuire, P. C., McKinley, G. A., Meyer, G.,
625 Morgan, E. J., Munro, D. R., Nakaoka, S.-I., Niwa, Y., O’Brien, K. M., Olsen, A., Omar, A. M., Ono, T., Paulsen,
626 M., Pierrot, D., Pockock, K., Poulter, B., Powis, C. M., Rehder, G., Resplandy, L., Robertson, E., Rödenbeck, C.,
627 Rosan, T. M., Schwinger, J., Séférian, R., et al.: Global Carbon Budget 2023, *Earth Syst. Sci. Data*, 15, 5301–
628 5369, <https://doi.org/10.5194/essd-15-5301-2023>, 2023.
- 629 Frölicher, T. L., Sarmiento, J. L., Paynter, D. J., Dunne, J. P., Krasting, J. P., and Winton, M.: Dominance of the
630 Southern Ocean in Anthropogenic Carbon and Heat Uptake in CMIP5 Models, *J. Clim.*, 28, 862–886,
631 <https://doi.org/10.1175/JCLI-D-14-00117.1>, 2015.
- 632 Giddy, I. S., Nicholson, S.-A., Queste, B. Y., Thomalla, S., and Swart, S.: Sea-Ice Impacts Inter-Annual Variability
633 of Phytoplankton Bloom Characteristics and Carbon Export in the Weddell Sea, *Geophys. Res. Lett.*, 50,
634 e2023GL103695, <https://doi.org/10.1029/2023GL103695>, 2023.
- 635 Giunta, V., & Ward, B. (2022). Ocean mixed layer depth from dissipation. *Journal of Geophysical Research:*
636 *Oceans*, 127, e2021JC017904. <https://doi.org/10.1029/2021JC017904>
- 637 Global Ocean Physics Analysis and Forecast:
638 https://data.marine.copernicus.eu/product/GLOBAL_ANALYSISFORECAST_PHY_001_024/description, last
639 access: 10 July 2024.



- 640 Global Ocean Physics Reanalysis:
641 https://data.marine.copernicus.eu/product/GLOBAL_MULTIYEAR_PHY_001_030/description, last access: 10
642 July 2024.
- 643 Global Total (COPERNICUS-GLOBCURRENT), Ekman and Geostrophic currents at the Surface and 15m:
644 https://data.marine.copernicus.eu/product/MULTIOBS_GLO_PHY_MYNRT_015_003/description, last access:
645 10 July 2024.
- 646 Gregor, L., Ryan-Keogh, T. J., Nicholson, S.-A., du Plessis, M., Giddy, I., and Swart, S.: GliderTools: A Python
647 Toolbox for Processing Underwater Glider Data, *Front. Mar. Sci.*, 6, <https://doi.org/10.3389/fmars.2019.00738>,
648 2019.
- 649 Gruber, N., Landschützer, P., and Lovenduski, N. S.: The Variable Southern Ocean Carbon Sink, *Annu. Rev. Mar.*
650 *Sci.*, 11, 159–186, <https://doi.org/10.1146/annurev-marine-121916-063407>, 2019.
- 651 Hauck, J., Völker, C., Wolf-Gladrow, D. A., Laufkötter, C., Vogt, M., Aumont, O., Bopp, L., Buitenhuis, E. T.,
652 Doney, S. C., Dunne, J., Gruber, N., Hashioka, T., John, J., Quéré, C. L., Lima, I. D., Nakano, H., Séférian, R.,
653 and Totterdell, I.: On the Southern Ocean CO₂ uptake and the role of the biological carbon pump in the 21st
654 century, *Glob. Biogeochem. Cycles*, 29, 1451–1470, <https://doi.org/10.1002/2015GB005140>, 2015.
- 655 Hauck, J., Nissen, C., Landschützer, P., Rödenbeck, C., Bushinsky, S., and Olsen, A.: Sparse observations induce
656 large biases in estimates of the global ocean CO₂ sink: an ocean model subsampling experiment, *Philos. Trans.*
657 *R. Soc. Math. Phys. Eng. Sci.*, 381, 20220063, <https://doi.org/10.1098/rsta.2022.0063>, 2023.
- 658 Henley, S. F., Cavan, E. L., Fawcett, S. E., Kerr, R., Monteiro, T., Sherrell, R. M., Bowie, A. R., Boyd, P. W.,
659 Barnes, D. K. A., Schloss, I. R., Marshall, T., Flynn, R., and Smith, S.: Changing Biogeochemistry of the Southern
660 Ocean and Its Ecosystem Implications, *Front. Mar. Sci.* 7, 581, <https://doi.org/10.3389/fmars.2020.00581>, 2020.
- 661 Holte, J. and Talley, L.: A New Algorithm for Finding Mixed Layer Depths with Applications to Argo Data and
662 Subantarctic Mode Water Formation*, *J. Atmospheric Ocean. Technol.*, 26, 1920–1939,
663 <https://doi.org/10.1175/2009JTECHO543.1>, 2009.
- 664 Laws, E. A.: Photosynthetic quotients, new production and net community production in the open ocean, *Deep*
665 *Sea Res. Part Oceanogr. Res. Pap.*, 38, 143–167, [https://doi.org/10.1016/0198-0149\(91\)90059-O](https://doi.org/10.1016/0198-0149(91)90059-O), 1991.
- 666 Lee, K., Tong, L. T., Millero, F. J., Sabine, C. L., Dickson, A. G., Goyet, C., Park, G.-H., Wanninkhof, R., Feely,
667 R. A., and Key, R. M.: Global relationships of total alkalinity with salinity and temperature in surface waters of
668 the world’s oceans, *Geophys. Res. Lett.*, 33, L19605, <https://doi.org/10.1029/2006GL027207>, 2006.
- 669 Lueker, T. J., Dickson, A. G., and Keeling, C. D.: Ocean pCO₂ calculated from dissolved inorganic carbon,
670 alkalinity, and equations for K₁ and K₂: validation based on laboratory measurements of CO₂ in gas and seawater
671 at equilibrium, *Mar. Chem.*, 70, 105–119, [https://doi.org/10.1016/S0304-4203\(00\)00022-0](https://doi.org/10.1016/S0304-4203(00)00022-0), 2000.
- 672 Mayot, N., Le Quéré, C., Rödenbeck, C., Bernardello, R., Bopp, L., Djeutchouang, L. M., Gehlen, M., Gregor, L.,
673 Gruber, N., Hauck, J., Iida, Y., Ilyina, T., Keeling, R. F., Landschützer, P., Manning, A. C., Patara, L., Resplandy,
674 L., Schwinger, J., Séférian, R., Watson, A. J., Wright, R. M., and Zeng, J.: Climate-driven variability of the
675 Southern Ocean CO₂ sink, *Philos. Trans. R. Soc. Math. Phys. Eng. Sci.*, 381, 20220055,
676 <https://doi.org/10.1098/rsta.2022.0055>, 2023.
- 677 McClish, S. and Bushinsky, S. M.: Majority of Southern Ocean Seasonal Sea Ice Zone Bloom Net Community
678 Production Precedes Total Ice Retreat, *Geophys. Res. Lett.*, 50, e2023GL103459,
679 <https://doi.org/10.1029/2023GL103459>, 2023.
- 680 Meijers, A. J. S., Le Quéré, C., Monteiro, P. M. S., and Sallée, J.-B.: Heat and carbon uptake in the Southern
681 Ocean: the state of the art and future priorities, *Philos. Trans. R. Soc. Math. Phys. Eng. Sci.*, 381, 20220071,
682 <https://doi.org/10.1098/rsta.2022.0071>, 2023.
- 683 Merlivat, L., Boutin, J., and d’Ovidio, F.: Carbon, oxygen and biological productivity in the Southern Ocean in
684 and out the Kerguelen plume: CARIOCA drifter results, *Biogeosciences*, 12, 3513–3524,
685 <https://doi.org/10.5194/bg-12-3513-2015>, 2015.



- 686 Mongwe, P., Gregor, L., Tjiputra, J., Hauck, J., Ito, T., Danek, C., Vichi, M., Thomalla, S., and Monteiro, P. M.
687 S.: Projected poleward migration of the Southern Ocean CO₂ sink region under high emissions, *Commun. Earth*
688 *Environ.*, 5, 1–13, <https://doi.org/10.1038/s43247-024-01382-y>, 2024.
- 689 Naëck, K., Boutin, J., Beaumont, L., Lourenco, A., and Sallée, J.-B.: CARIOCA observations - SO-CHIC Cruise
690 2022, <https://doi.org/10.17882/100800>, 2024.
- 691 Nicholson, S.-A., Whitt, D. B., Fer, I., Du Plessis, M. D., Lebéhot, A. D., Swart, S., Sutton, A. J., and Monteiro,
692 P. M. S.: Storms drive outgassing of CO₂ in the subpolar Southern Ocean, *Nat. Commun.*, 13, 158,
693 <https://doi.org/10.1038/s41467-021-27780-w>, 2022.
- 694 OceanColour - CCI: <https://www.oceancolour.org/>, last access: 10 July 2024.
- 695 Ogundare, M. O., Fransson, A., Chierici, M., Joubert, W. R., and Roychoudhury, A. N.: Variability of Sea-Air
696 Carbon Dioxide Flux in Autumn Across the Weddell Gyre and Offshore Dronning Maud Land in the Southern
697 Ocean, *Front. Mar. Sci.*, 7, 614263, <https://doi.org/10.3389/fmars.2020.614263>, 2021.
- 698 OSCAR third degree resolution ocean surface currents | PO.DAAC / JPL / NASA:
699 https://podaac.jpl.nasa.gov/dataset/OSCAR_L4_OC_third-deg, last access: 10 July 2024.
- 700 Park, Y. -H., Park, T., Kim, T. -W., Lee, S. -H., Hong, C. -S., Lee, J. -H., Rio, M. -H., Pujol, M. -I., Ballarotta,
701 M., Durand, I., and Provost, C.: Observations of the Antarctic Circumpolar Current Over the Udintsev Fracture
702 Zone, the Narrowest Choke Point in the Southern Ocean, *J. Geophys. Res. Oceans*, 124, 4511–4528,
703 <https://doi.org/10.1029/2019JC015024>, 2019.
- 704 Pellichero, V., Boutin, J., Claustre, H., Merlivat, L., Sallée, J., and Blain, S.: Relaxation of Wind Stress Drives the
705 Abrupt Onset of Biological Carbon Uptake in the Kerguelen Bloom: A Multisensor Approach, *Geophys. Res.*
706 *Let.*, 47, <https://doi.org/10.1029/2019GL085992>, 2020.
- 707 Person, R., Aumont, O., Madec, G., Vancoppenolle, M., Bopp, L., and Merino, N.: Sensitivity of ocean
708 biogeochemistry to the iron supply from the Antarctic Ice Sheet explored with a biogeochemical model,
709 *Biogeosciences*, 16, 3583–3603, <https://doi.org/10.5194/bg-16-3583-2019>, 2019.
- 710 Rousselet L., d’Ovidio F., Izard L., Della Penne A., Petrenko A., Barrillon S., Nencioli F., Doglioli A., (submitted,
711 JTECH-D-240071), A Software Package for an Adaptive Satellite-based Sampling for Oceanographic cruises
712 (SPASSOv2.0): tracking fine scale features for physical and biogeochemical studies.
- 713 Sabine, C. L., Feely, R. A., Gruber, N., Key, R. M., Lee, K., Bullister, J. L., Wanninkhof, R., Wong, C. S., Wallace,
714 D. W. R., Tilbrook, B., Millero, F. J., Peng, T.-H., Kozyr, A., Ono, T., and Rios, A. F.: The Oceanic Sink for
715 Anthropogenic CO₂, *Science*, 305, 367–371, <https://doi.org/10.1126/science.1097403>, 2004.
- 716 Sanial, V., van Beek, P., Lansard, B., d’Ovidio, F., Kestenare, E., Souhaut, M., Zhou, M., and Blain, S. (2014).
717 Study of the phytoplankton plume dynamics off the Crozet Islands (Southern Ocean): A geochemical-physical
718 coupled approach. *Journal of Geophysical Research: Oceans* 119, 2227–2237.
- 719 Steiger, N., Sallée, J., Ward, B., Azevedo, A., Binase, Z., Ten Doeschat, A., Els, H., Hamnca, S., Jacobs, L.,
720 Katsoulis, M., Lavanchy, S., Lavis, C., Lourenco, A., Du Plessis, M., Rosenthal, H., Soares, B., and Spira, T.:
721 CTD observation - SO-CHIC Cruise 2022, <https://doi.org/10.17882/95314>, 2022.
- 722 Sergi, S., Baudena, A., Cotté, C., Ardyna, M., Blain, S., and d’Ovidio, F.: Interaction of the Antarctic Circumpolar
723 Current With Seamounts Fuels Moderate Blooms but Vast Foraging Grounds for Multiple Marine Predators, *Front.*
724 *Mar. Sci.*, 7, 416, <https://doi.org/10.3389/fmars.2020.00416>, 2020.
- 725 Smith, R. M. and Bigg, G. R.: Impact of Giant Iceberg A68A on the Physical Conditions of the Surface South
726 Atlantic, Derived Using Remote Sensing, *Geophys. Res. Lett.*, 50, e2023GL104028,
727 <https://doi.org/10.1029/2023GL104028>, 2023.
- 728 Sutherland, G., G. Reverdin, L. Marié, and B. Ward (2014), Mixed and mixing layer depths in the ocean surface
729 boundary layer under conditions of diurnal stratification, *Geophys. Res. Lett.*, 41, doi:10.1002/2014GL061939.
- 730 Swart, S., du Plessis, M., Giddy, I., Edholm, J., Spira, T., Biddle, L., and Rosenthal, H. S.: Dataset from



- 731 autonomous assets collected during the SO-CHIC field campaign in the Southern Ocean (1),
732 <https://doi.org/10.5281/ZENODO.11059425>, 2024.
- 733 Szekely, T., Gourrion, J., Pouliquen, S., and Reverdin, G.: CORA, Coriolis Ocean Dataset for Reanalysis,
734 <https://doi.org/10.17882/46219>, 2024.
- 735 Takahashi, T., Sutherland, S. C., Sweeney, C., Poisson, A., Metzl, N., Tilbrook, B., Bates, N., Wanninkhof, R.,
736 Feely, R. A., Sabine, C., Olafsson, J., and Nojiri, Y.: Global sea-air CO₂ flux based on climatological surface
737 ocean pCO₂, and seasonal biological and temperature effects, *Deep Sea Res. Part II Top. Stud. Oceanogr.*, 49,
738 1601–1622, [https://doi.org/10.1016/S0967-0645\(02\)00003-6](https://doi.org/10.1016/S0967-0645(02)00003-6), 2002.
- 739 Takahashi, T., Sweeney, C., Hales, B., Chipman, D. W., Newberger, T., Goddard, J. G., Iannuzzi, R. A., and
740 Sutherland, S. C.: The Changing Carbon Cycle in the Southern Ocean, *Oceanography*, 25, 26–37, 2012.
- 741 The SO-CHIC consortium, Sallée, J. B., Abrahamsen, E. P., Allaire, C., Auger, M., Ayres, H., Badhe, R., Boutin,
742 J., Brearley, J. A., De Lavergne, C., Ten Doeschate, A. M. M., Droste, E. S., Du Plessis, M. D., Ferreira, D., Giddy,
743 I. S., Gülk, B., Gruber, N., Hague, M., Hoppema, M., Josey, S. A., Kanzow, T., Kimmritz, M., Lindeman, M. R.,
744 Llanillo, P. J., Lucas, N. S., Madec, G., Marshall, D. P., Meijers, A. J. S., Meredith, M. P., Mohrmann, M.,
745 Monteiro, P. M. S., Mosneron Dupin, C., Naeck, K., Narayanan, A., Naveira Garabato, A. C., Nicholson, S.-A.,
746 Novellino, A., Ódalen, M., Østerhus, S., Park, W., Patmore, R. D., Piedagnel, E., Roquet, F., Rosenthal, H. S.,
747 Roy, T., Saurabh, R., Silvy, Y., Spira, T., Steiger, N., Styles, A. F., Swart, S., Vogt, L., Ward, B., and Zhou, S.:
748 Southern ocean carbon and heat impact on climate, *Philos. Trans. R. Soc. Math. Phys. Eng. Sci.*, 381, 20220056,
749 <https://doi.org/10.1098/rsta.2022.0056>, 2023.
- 750 Thomalla, S. J., Moutier, W., Ryan-Keogh, T. J., Gregor, L., and Schütt, J.: An optimized method for correcting
751 fluorescence quenching using optical backscattering on autonomous platforms: Method for correcting fluorescence
752 quenching, *Limnol. Oceanogr. Methods*, 16, 132–144, <https://doi.org/10.1002/lom3.10234>, 2018.
- 753 Vernet, M., Geibert, W., Hoppema, M., Brown, P. J., Haas, C., Hellmer, H. H., Jokat, W., Jullion, L., Mazloff, M.,
754 Bakker, D. C. E., Brearley, J. A., Croot, P., Hattermann, T., Hauck, J., Hillenbrand, C. -D., Hoppe, C. J. M., Huhn,
755 O., Koch, B. P., Lechtenfeld, O. J., Meredith, M. P., Naveira Garabato, A. C., Nöthig, E. -M., Peeken, I., Rutgers
756 Van Der Loeff, M. M., Schmidtko, S., Schröder, M., Strass, V. H., Torres-Valdés, S., and Verdy, A.: The Weddell
757 Gyre, Southern Ocean: Present Knowledge and Future Challenges, *Rev. Geophys.*, 57, 623–708,
758 <https://doi.org/10.1029/2018RG000604>, 2019.
- 759 Wang, J., Luo, H., Yang, Q., Liu, J., Yu, L., Shi, Q., and Han, B.: An Unprecedented Record Low Antarctic Sea-
760 ice Extent during Austral Summer 2022, *Adv. Atmospheric Sci.*, 39, 1591–1597, <https://doi.org/10.1007/s00376-022-2087-1>, 2022.
- 762 Wanninkhof, R.: Relationship between wind speed and gas exchange over the ocean, *J. Geophys. Res.*, 97, 7373,
763 <https://doi.org/10.1029/92JC00188>, 1992.
- 764 Wanninkhof, R.: Relationship between wind speed and gas exchange over the ocean revisited: Gas exchange and
765 wind speed over the ocean, *Limnol. Oceanogr. Methods*, 12, 351–362, <https://doi.org/10.4319/lom.2014.12.351>,
766 2014.
- 767 Ward, B., Azevedo, A., Binase, Z., ten Doeschate, A., Els, H., Hamna, S., Jacobs, L., Katsoulis, M., Lavanchy,
768 S., Lavis, C., Lourenco, A., du Plessis, M., Rosenthal, H., Sallee, J.-B., Soares, B., Spira, T., and Steiger, N.:
769 SOCHIC cruise report, Zenodo, <https://doi.org/10.5281/ZENODO.6948850>, 2022.
- 770 Ward, B., Naëck, K., Boutin, J., Sallée, J.-B., Jacobs, L., and Steiger, N.: TSG observations - SO-CHIC Cruise
771 2022, <https://doi.org/10.17882/100905>, 2024.
- 772 Weiss, R. F.: Carbon dioxide in water and seawater: the solubility of a non-ideal gas, *Mar. Chem.*, 2, 203–215,
773 [https://doi.org/10.1016/0304-4203\(74\)90015-2](https://doi.org/10.1016/0304-4203(74)90015-2), 1974.